

# 000 001 002 003 004 005 PRISM: PROGRESSIVE ROBUST LEARNING FOR 006 OPEN-WORLD CONTINUAL CATEGORY DISCOVERY 007 008 009

010 **Anonymous authors**  
011 Paper under double-blind review  
012  
013  
014  
015  
016  
017  
018  
019  
020  
021  
022  
023  
024  
025  
026  
027  
028  
029  
030

## ABSTRACT

031 Continual Category Discovery (CCD) aims to leverage models trained on known  
032 categories to automatically discover novel category concepts from continuously  
033 arriving streams of unlabeled data, while retaining the ability to recognize pre-  
034 viously known classes. Despite recent progress, existing methods often assume  
035 that data across all stages are drawn from a single, stationary distribution—a  
036 condition rarely satisfied in open-world scenarios. In this paper, we challenge  
037 this stationary-distribution assumption by introducing the Open-World Continual  
038 Category Discovery (OW-CCD) setting. We address this challenge with PRISM  
039 (Progressive Robust dIscovery under StreaMing data), an adaptive continual dis-  
040 covery framework consisting of three key components. First, inspired by spectral  
041 properties, we develop a high-frequency-driven category separation technique that  
042 exploits high-frequency components—preserving more global information—to  
043 distinguish known from unknown categories. Second, for known categories, we  
044 design a sparse assignment matching strategy, which performs proximal sparse  
045 sample-to-label matching to assign reliable cluster labels to known-class sam-  
046 ples. Finally, to better recognize novel categories, we propose an invariant knowl-  
047 edge transfer module that enforces domain-invariant category relation consistency,  
048 thereby facilitating robust knowledge transfer from known to unknown classes un-  
049 der domain shifts. Extensive experiments on the SSB-C and DomainNet bench-  
050 marks demonstrate that our method significantly outperforms state-of-the-art CCD  
051 approaches, highlighting its effectiveness and superiority.  
052

## 1 INTRODUCTION

053 Visual concepts in the real world are open-ended and continually evolving, far exceeding any pre-  
054 defined category set. Although deep learning has achieved remarkable progress in visual recognition,  
055 most advances rely on closed-world assumptions—models are trained on fixed label spaces and  
056 therefore struggle when encountering previously unseen categories. Humans, by contrast, naturally  
057 generalize from prior knowledge to organize and recognize new concepts. This discrepancy has led  
058 to growing interest in category discovery (Vaze et al., 2022; Han et al., 2021; Wen et al., 2023).

059 Early studies formulated this task as Novel Class Discovery (NCD) (Han et al., 2021), where all  
060 unlabeled samples belong to novel categories. To better reflect realistic conditions, Generalized  
061 Category Discovery (GCD) (Vaze et al., 2022; Wen et al., 2023) extended this setting by allowing  
062 unlabeled data to contain a mixture of known and unknown classes, requiring models to both identify  
063 known classes and cluster new ones. However, both NCD and GCD are built upon static datasets and  
064 assume simultaneous access to labeled and unlabeled data. These assumptions diverge from real-  
065 world conditions, where data typically arrive as continuously evolving, unlabelled streams. As a  
066 result, NCD and GCD overlook the dynamic nature of open environments and fall short of modeling  
067 realistic data-stream scenarios.

068 To close this gap, the community has recently moved toward Continual Category Discovery  
069 (CCD) (Park et al., 2024; Cendra et al., 2024), which integrates continual learning with category  
070 discovery. CCD aims to progressively identify emerging categories while preventing catastrophic  
071 forgetting of previous knowledge. Despite this progress, existing CCD settings commonly assume  
072 that data at each stage comes from a single, fixed domain—an assumption rarely met in open envi-  
073 ronments. In practical scenarios, samples may originate from diverse sources or shift across domains

054 while new categories appear. For example, an online platform may continuously receive animal images  
 055 from different cameras or users; as the domain (e.g., lighting, style, device) changes, rare  
 056 species can emerge concurrently with existing categories.

057 Motivated by these limitations, we propose a more realistic setting called **Open-World Continual**  
 058 **Category Discovery (OW-CCD)**. In OW-CCD, models must automatically discover known and  
 059 unknown categories from unlabeled streams without assuming domain consistency. This introduces  
 060 several challenges. First, it is difficult to preserve recognition ability for known categories under  
 061 distribution shifts, as existing CCD methods are not designed to handle domain variations. Second,  
 062 the model must continually discover emerging categories in dynamic, non-stationary streams. Tra-  
 063 ditional domain adaptation techniques are unsuitable, as they often assume overlapping label spaces;  
 064 naïve alignment may even cause negative transfer and suppress novel-category discovery. Moreover,  
 065 most adaptation methods focus on aligning known classes, offering little guidance for discovering  
 066 unseen ones.

067 To address these challenges, we introduce **PRISM**  
 068 (**P**rogressive **R**obust **I**l<sub>s</sub>**o****c**o**r**u**s** **S**tream**I**ng data), a new adaptive divide-and-conquer frame-  
 069 work for OW-CCD. Our design is inspired by spec-  
 070 tral analysis (Fig. 1(a–c)): high-frequency compo-  
 071 nents tend to capture domain-invariant global se-  
 072 mantics (e.g., structures), whereas low-frequency  
 073 components encode domain-dependent details (e.g.,  
 074 style). Leveraging this insight, we develop a high-  
 075 frequency-driven category separation module to dis-  
 076 tinguish known from unknown samples under do-  
 077 main shift. To ensure reliable recognition of known  
 078 categories, we further propose a sparse assignment  
 079 matching module based on proximal optimal trans-  
 080 port, producing stable and sparse pseudo-labels. Fi-  
 081 nally, following the core principle of category dis-  
 082 covery—transferring knowledge from known to un-  
 083 known classes through semantic relations—we in-  
 084 troduce an invariant knowledge transfer (IKT) mod-  
 085 ule. Instead of relying on domain-specific cues that  
 086 may distort associations, IKT represents the rela-  
 087 tions between known and unknown classes as rank-  
 088 ing permutations. These permutations are converted  
 089 into ranking probability distributions and enforced  
 090 to remain consistent across domains. This rank-based formulation ensures that semantically closer  
 091 classes contribute stronger knowledge transfer; for instance, in CUB, closely related bird species  
 092 such as Indigo Bunting and Lazuli Bunting share meaningful high-level semantics despite subtle  
 093 visual differences. Maintaining these relationships across domains enables stable transfer and facil-  
 094 itates robust discovery of novel categories.

095 In summary, our contributions are as follows: (1) we introduce the Open-World Continual Category  
 096 Discovery (OW-CCD) setting and present PRISM, an adaptive divide-and-conquer framework; (2)  
 097 we propose a high-frequency-driven category separation strategy to distinguish known and unknown  
 098 samples under domain shifts; (3) we design a sparse assignment matching module based on prox-  
 099 imal optimal transport for reliable pseudo-labeling of known categories; (4) we develop an invariant  
 100 knowledge transfer module that preserves semantic relations between known and unknown cate-  
 101 gories across domains for stable discovery; and (5) through extensive evaluation on the SSB-C and  
 102 DomainNet benchmarks, we demonstrate that PRISM achieves strong effectiveness and robustness,  
 103 consistently outperforming state-of-the-art CCD approaches.

## 104 2 RELATED WORK

105 **Category Discovery** Category discovery aims to leverage knowledge from labeled classes to iden-  
 106 tify novel concepts in unlabeled data. Novel Class Discovery (NCD) was introduced to address sce-

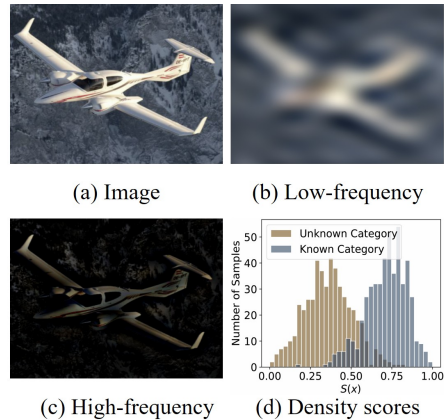


Figure 1: (a–c) Visualization of low-frequency and high-frequency components of the images. (d) Visualization of the density scores  $S(x)$ , where the density distribution exhibits a clear bimodal pattern corresponding to known and unknown samples.

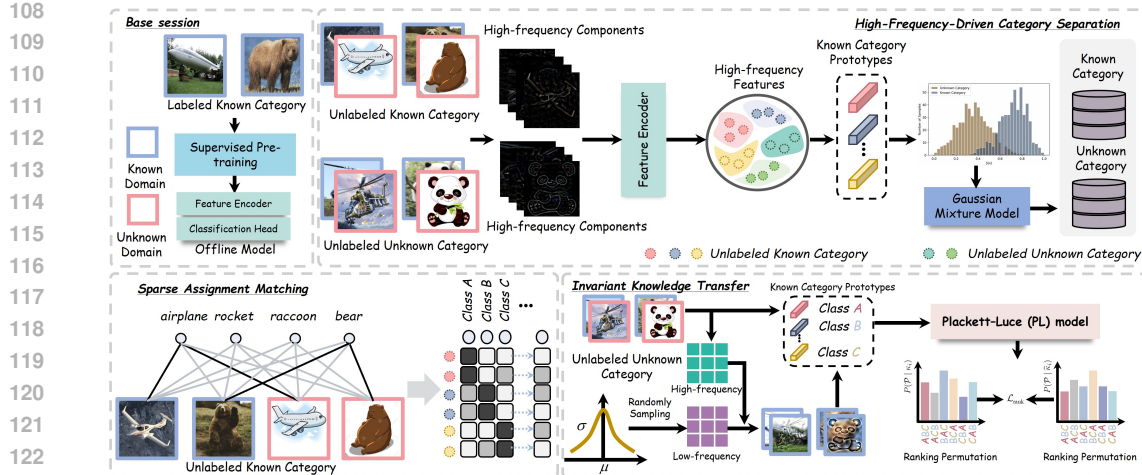


Figure 2: The overall framework of our proposed method.

scenarios where all unlabeled samples belong to unseen categories. Early methods adopted two-stage pipelines, such as AutoNovel (Han et al., 2021), which transfers knowledge through self-supervised learning with ranking statistics. In contrast, unified end-to-end approaches (Fini et al., 2021) directly integrate representation learning and clustering into a single stage. Later extensions address sample imbalance by designing self-cooperation mechanisms that leverage both known and novel representations for mutual learning (Wang et al., 2024c), or enhance class-level knowledge transfer through symmetric relationship modeling and pairwise consistency constraints (Zhou & Chen, 2025). Generalized Category Discovery (GCD) relaxes this setting by mixing known and unknown categories. Early frameworks combined supervised and unsupervised contrastive learning with clustering (Vaze et al., 2022), while SimGCD (Wen et al., 2023) introduced a parametric classifier for efficiency. More recent work explores hierarchical modeling (Liu et al., 2025b), prototype-based learning (Ma et al., 2025), and reciprocal learning with distribution regularization (Liu et al., 2025a). Beyond these directions, some studies investigate domain-level extensions, addressing category discovery under domain shifts (Wang et al., 2024a; Rongali et al., 2024). Continuous Category Discovery (CCD) further considers streaming settings. Methods such as grow and merge (Zhang et al., 2022), energy-guided discovery (Park et al., 2024), Gaussian mixture prompting (Cendra et al., 2024), and Bayesian inference (Dai & Chauhan, 2025) have been proposed to tackle class discovery in streaming data, though they often operate under the simplifying assumption of single-domain streams.

**Domain Adaptation** Domain adaptation tackles distribution gaps between labeled source and target domains. Unsupervised domain adaptation (UDA) leverages labeled source and unlabeled target data, typically by learning domain-invariant representations. Discrepancy-based methods minimize moment mismatches (Sun & Saenko, 2016; Long et al., 2015; Tzeng et al., 2014), while adversarial approaches employ domain discriminators (Saito et al., 2018a; Sankaranarayanan et al., 2018). Transformer-based backbones (Dosovitskiy et al., 2020) have also been explored with attention-driven alignment (Sun et al., 2022; Xu et al., 2021). Source-Free Domain Adaptation (SFDA) removes source data access. Representative works include prototype transfer (Chidlovskii et al., 2016), iterative pseudo-labeling (Liang et al., 2019), SHOT (Krause et al., 2010; Shi & Sha, 2012), and neighborhood regularization (Yang et al., 2021). Beyond this, Open-Set Domain Adaptation (OSDA) addresses unknown target categories. Strategies include confidence thresholding (Saito et al., 2018b), progressive separation (Liu et al., 2019), and causal adjustment (Li et al., 2023b). While OSDA extends domain adaptation to more realistic scenarios, most existing methods remain centered on classifying known categories and pay limited attention to systematically exploring the unknown label space.

162 **3 METHODOLOGY**  
 163

164 **3.1 PROBLEM STATEMENT**  
 165

166 Open-World Continual Category Discovery (OW-CCD) involves one base learning session followed  
 167 by  $T$  online continual discovery sessions. In the base session, we are provided with a labeled dataset  
 168  $\mathcal{D}^l = \{(x_i, y_i)\}_{i=1}^{N^l}$  consisting of  $N^l$  labeled samples drawn from a known category space  $\mathcal{C}^l$ . In  
 169 each subsequent online discovery session, an unlabeled data stream  $\mathcal{D}_t^u = \{x_i\}_{i=1}^{N_t^u}$  is introduced in-  
 170 crementally. This stream not only contains samples from the previously seen known categories, but  
 171 also includes samples from novel categories  $\mathcal{C}_t^u$  in session  $t$ . Moreover, these samples may originate  
 172 from domains that differ from the domain distributions observed in the base session, thus introducing  
 173 additional domain shift. The goal of OW-CCD is to enable the model to robustly discover novel  
 174 concepts from the dynamic unlabeled data stream in an online manner, while simultaneously main-  
 175 taining recognition capability for known categories and alleviating the impact of distribution shifts  
 176 as much as possible.

177 Fig. 2 illustrates the overall framework of our proposed PRISM method. In the base session, we first  
 178 pre-train a model  $\theta = \{f, g\}$  on the labeled dataset using cross-entropy loss, where  $f(\cdot)$  denotes  
 179 the feature extractor and  $g(\cdot)$  is the classifier head. This provides discriminative representations as  
 180 a foundation for subsequent discovery. In the online discovery stage, we then introduce three key  
 181 innovations. First, the High-Frequency-Driven Category Separation (HCS) is employed to automati-  
 182 cally separate known and unknown categories by exploiting high-frequency information in images.  
 183 Second, the Sparse Assignment Matching (SAM) module assigns reliable cluster labels to samples  
 184 from known categories. Finally, the Invariant Knowledge Transfer (IKT) module captures robust  
 185 category associations across different domains, thereby enabling stable and effective novel category  
 186 discovery.

187 **3.2 HIGH-FREQUENCY-DRIVEN CATEGORY SEPARATION (HCS)**  
 188

189 Since direct distribution alignment may lead to negative transfer, we adopt a divide-and-conquer  
 190 strategy. Below, we first describe how to extract the high- and low-frequency components of images,  
 191 and then employ the HCS module for category separation. Given an input image  $x_i \in \mathbb{R}^{H \times W \times C}$ ,  
 192 where  $H$ ,  $W$ , and  $C$  denote the height, width, and number of channels, respectively, we first trans-  
 193 form it into the frequency domain using the Discrete Fourier Transform (DFT):

$$194 \quad \mathcal{F}(x_i)(u, v, c) = \sum_{h=0}^{H-1} \sum_{w=0}^{W-1} x_i(h, w, c) e^{-j2\pi \left( \frac{hu}{H} + \frac{wv}{W} \right)}, \quad (1)$$

197 where  $j^2 = -1$ ,  $u$  and  $v$  denote the spatial frequency coordinates, and  $c$  indexes the RGB channels.  
 198 Following common practice, the low-frequency components are shifted to the center of the spectrum  
 199 for convenience. To separate low- and high-frequency information, we construct a binary mask  
 200  $M \in \mathbb{R}^{r \times r}$ :

$$201 \quad M_{u,v} = \begin{cases} 1, & \text{if } \max(|u - \frac{H}{2}|, |v - \frac{W}{2}|) \leq r \cdot \frac{\min(H, W)}{2}, \\ 0, & \text{otherwise,} \end{cases} \quad (2)$$

204 where  $r$  controls the relative size of the mask. The low- and high-pass frequency components are  
 205 then obtained as:

$$206 \quad \mathcal{F}^l(x_i) = M \odot \mathcal{F}(x_i), \quad \mathcal{F}^h(x_i) = (I - M) \odot \mathcal{F}(x_i), \quad (3)$$

207 where  $\odot$  denotes element-wise multiplication, and  $\mathcal{F}^l$  and  $\mathcal{F}^h$  are the masked low- and high-  
 208 frequency spectra obtained from the DFT  $\mathcal{F}(x_i)$ . Finally, inverse DFT is applied to recover spatial  
 209 representations of low- and high-frequency images:  $x_i^l = \mathcal{F}^{-1}(\mathcal{F}^l(x_i))$ ,  $x_i^h = \mathcal{F}^{-1}(\mathcal{F}^h(x_i))$ .

210 We focus on the high-frequency component  $x_i^h$  of the unlabeled data, as high-frequency cues often  
 211 contain discriminative structural information that helps distinguish known from unknown categories  
 212 (see Fig. 1(a-c)). These components are fed into the pre-trained feature extractor  $f$  from the pre-  
 213 vious stage to obtain high-frequency representations. Based on these representations, we define a

214 density scoring function:  $S(x) = \nu \left( \max_c \frac{f(x^h) \cdot e_c}{\|f(x^h)\| \cdot \|e_c\|} \right)$ , where  $e_c$  denotes the prototype of the

known class  $c$  from the previous stage, and  $\nu(\cdot)$  is a min–max normalization mapping scores to  $[0, 1]$ . Intuitively,  $S(x)$  measures the maximum similarity between the high-frequency representation of an unlabeled sample and known category prototypes: larger values indicate that the sample is closer to known classes, while smaller values imply it may belong to an unknown class. As shown in Fig. 1(d), we empirically observe that the distribution of  $S(x)$  often exhibits a bimodal shape, corresponding to known and unknown samples, respectively. To automatically separate them, we model the distribution of  $S(x)$  using a two-component Gaussian Mixture Model (GMM):  $P(x) = \pi(x) \mathcal{N}(x|\mu_{\text{kno}}, \sigma_{\text{kno}}^2) + (1 - \pi(x)) \mathcal{N}(x|\mu_{\text{unk}}, \sigma_{\text{unk}}^2)$ , where  $\pi(x)$  is the posterior probability of being assigned to the known component, estimated using the EM algorithm.  $\mathcal{N}(x | \mu, \sigma^2)$  denotes a Gaussian distribution with mean  $\mu$  and variance  $\sigma^2$ , and  $(\mu_{\text{kno}}, \sigma_{\text{kno}}^2)$  and  $(\mu_{\text{unk}}, \sigma_{\text{unk}}^2)$  correspond to the parameters of the known and unknown components, respectively. Finally, at each online session  $t$ , we split the incoming data stream  $\mathcal{D}_t^u$  into known and unknown subsets:

$$\mathcal{D}_{t,\text{kno}}^u = \{x \mid x \in \mathcal{D}_t^u \wedge \pi(x) \geq 0.5\}, \quad \mathcal{D}_{t,\text{unk}}^u = \{x \mid x \in \mathcal{D}_t^u \wedge \pi(x) < 0.5\}. \quad (4)$$

This separation provides a reliable mechanism for dynamically identifying known-like and unknown-like samples, which lays the foundation for subsequent discriminative learning and novel category discovery.

### 3.3 SPARSE ASSIGNMENT MATCHING (SAM)

Since we have already obtained the known-category samples via the proposed HCS module, we next explore the possible labels for these known samples  $x_{\text{kno}} \in \mathcal{D}_{t,\text{kno}}^u$ . As  $x_{\text{kno}}$  shares the same semantic space with the known prototypes from the previous stage, domain adaptation techniques can be employed to uncover the latent alignment. In this process, Optimal Transport (OT) provides a powerful tool to automatically discover proper sample–prototype correspondences across domains, thereby alleviating domain discrepancies (Courty et al., 2014; Flamary et al., 2016). However, directly solving the OT problem with linear programming incurs a prohibitive computational cost (Xu & Dan, 2025); even though the entropy regularization can improve efficiency, it usually yields overly dense transport plans, leading to inaccurate assignments as illustrated in Fig. 3(a). To overcome this limitation, we propose a Sparse Assignment Matching (SAM) scheme by incorporating an  $\ell_2$ -norm proximal term. The optimization objective is formulated as:

$$\min_{\gamma \in \Delta} \ell(\gamma) = \sum_{i=1}^{N_{t,\text{kno}}} \sum_{j=1}^{\mathcal{C}^{t-1}} \left[ \gamma_{ij} C_{ij} + \frac{\varepsilon}{2} (\gamma_{ij} - \gamma_{ij}^{(l)})^2 \right], \quad (5)$$

where  $N_{t,\text{kno}}$  denotes the number of samples in  $\mathcal{D}_{t,\text{kno}}^u$ .  $\mathcal{C}^{t-1}$  denotes the number of known classes from the previous stage. The cost matrix is defined as  $C_{ij} = -\log(g(f(x_{i,\text{kno})))_j)$ . A smaller value of  $C_{ij}$  indicates that sample  $x_{i,\text{kno}}$  has a higher probability of belonging to the  $j$ -th class, while a larger cost suggests a less plausible assignment. The second term  $\frac{\varepsilon}{2} \sum_{i,j} (\gamma_{ij} - \gamma_{ij}^{(l)})^2$  acts as an  $\ell_2$ -based proximal regularizer, which suppresses oscillations across iterations and enforces sparse and stable solutions. Meanwhile,  $\Delta = \left\{ \sum_{j=1}^{\mathcal{C}^{t-1}} \gamma_{ij} = \hat{a}_i = 1, \sum_{i=1}^{N_{t,\text{kno}}} \gamma_{ij} = \hat{b}_j = \frac{N_{t,\text{kno}}}{\mathcal{C}^{t-1}}, \gamma_{ij} \geq 0 \right\}$  is the feasible set. We initialize  $\gamma_{ij}^{(0)} = \frac{1}{\mathcal{C}^{t-1}}$  for the following iterations. To avoid directly handling the constrained problem, we first obtain the Fenchel–Legendre dual formulation of the original problem:

$$\max_{\psi, \varphi} \sum_{i=1}^{N_{t,\text{kno}}} \psi_i \hat{a}_i + \sum_{j=1}^{\mathcal{C}^{t-1}} \varphi_j \hat{b}_j - \frac{\varepsilon}{2} \sum_{i=1}^{N_{t,\text{kno}}} \sum_{j=1}^{\mathcal{C}^{t-1}} \left[ \frac{\psi_i + \varphi_j - \tilde{C}_{ij}}{\varepsilon} \right]_+^2, \quad (6)$$

where  $\varphi$  and  $\psi$  denote the Lagrange multipliers, and  $[z]_+^2 = (\max\{0, z\})^2$  denotes the truncated quadratic operator ensuring non-negativity.  $\tilde{C}_{ij} = C_{ij} - \varepsilon \gamma_{ij}^{(l)}$ . Note that the original con-

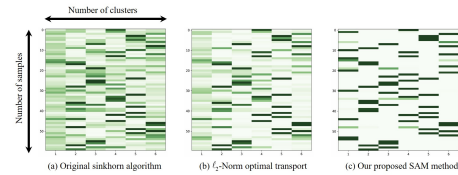


Figure 3: Toy illustration of our proposed SAM method. Conventional Sinkhorn and  $\ell_2$ -regularized solvers tend to produce smooth yet dense couplings, whereas the proposed SAM yields a sparser transport plan with better performance.

270 strained OT problem in Eq. (5) is transformed into an unconstrained optimization over  $(\psi, \varphi)$ ,  
 271 which is computationally more efficient. The detailed optimization procedure for solving  $\psi$  and  
 272  $\varphi$  is provided in the Appendix. Then the transport plan  $\gamma^{(l+1)}$  can be updated in closed form as:  
 273  $\gamma_{ij}^{(l+1)} = \max \left\{ 0, (\psi_i + \varphi_j + \varepsilon \gamma_{ij}^{(l)} - C_{ij}) / \varepsilon \right\}$ .  
 274

275 With the optimal transport plan  $\gamma^*$  obtained from sparse sample-prototype alignment, we assign  
 276 reliable pseudo labels to the known samples  $x_{\text{kno}} \in \mathcal{D}_{t, \text{kno}}^u$ . Moreover, compared with the standard  
 277  $\ell_2$ -regularized OT, the proposed SAM produces significantly sparser and clearer assignment pat-  
 278 terns, as depicted in Fig. 3(b)–(c), which contributes to more trustworthy pseudo-label generation.  
 279

### 280 3.4 INVARIANT KNOWLEDGE TRANSFER (IKT)

281 For unknown category discovery, we build on the core idea of category discovery—transferring cat-  
 282 egory knowledge from known to unknown classes by exploiting their semantic associations. Under  
 283 domain shift, however, such associations may be distorted by domain-specific style factors, lead-  
 284 ing the model to capture spurious rather than genuine relations. We argue that effective discovery  
 285 should instead depend on domain-invariant category associations that reflect stable semantic struc-  
 286 tures. To this end, we propose an *Invariant Knowledge Transfer* module, which explicitly models the  
 287 relationships between unknown samples and known prototypes across domains and enforces their  
 288 invariance, thereby facilitating the transfer of authentic semantic knowledge. Specifically, in each  
 289 previous stage we pre-compute the frequency-domain statistics of the known domain. For this pur-  
 290 pose, we apply the discrete Fourier transform as in Eq. (1) and decompose each spectrum into low-  
 291 and high-frequency components  $\{\mathcal{F}^l, \mathcal{F}^h\}$  according to Eq. (3). Inspired by recent works (Li et al.,  
 292 2022; Wang et al., 2022) that employ spatial feature statistics to characterize style, we characterize  
 293 the low-frequency spectrum by the channel-wise mean and standard deviation:

$$\mu(\mathcal{F}_i^l) = \frac{1}{HW} \sum_{u,v} \mathcal{F}_i^l(u, v, c), \quad \sigma(\mathcal{F}_i^l) = \frac{1}{HW} \sum_{u,v} [\mathcal{F}_i^l(u, v, c) - \mu(\mathcal{F}_i^l)]^2. \quad (7)$$

294 We assume that the distribution of these statistics follows a Gaussian distribution, and estimate their  
 295 variances across the data from the previous stage:

$$\Sigma_\mu^2(\mathcal{F}_i^l) = \frac{1}{N_{t-1}} \sum_{i=1}^{N_{t-1}} [\mu(\mathcal{F}_i^l) - \mathbb{E}[\mu(\mathcal{F}_i^l)]]^2, \quad \Sigma_\sigma^2(\mathcal{F}_i^l) = \frac{1}{N_{t-1}} \sum_{i=1}^{N_{t-1}} [\sigma(\mathcal{F}_i^l) - \mathbb{E}[\sigma(\mathcal{F}_i^l)]]^2, \quad (8)$$

296 where  $N_{t-1}$  denotes the number of samples from the previous stage. We then sample perturbed  
 297 low-frequency statistics from these Gaussian distributions:

$$\hat{\mu}(\mathcal{F}_i^l) = \mu(\mathcal{F}_i^l) + \epsilon_\mu \Sigma_\mu(\mathcal{F}_i^l), \quad \epsilon_\mu \sim \mathcal{N}(0, 1), \quad \hat{\sigma}(\mathcal{F}_i^l) = \sigma(\mathcal{F}_i^l) + \epsilon_\sigma \Sigma_\sigma(\mathcal{F}_i^l), \quad \epsilon_\sigma \sim \mathcal{N}(0, 1). \quad (9)$$

308 For an unknown sample  $x_{i, \text{unk}}^t$  in the current data stream, we extract its low-/high-frequency com-  
 309 ponents  $(\mathcal{F}_{i, \text{unk}}^l, \mathcal{F}_{i, \text{unk}}^h)$  via Eq. (3) and reconstruct the low-frequency spectrum with the sampled  
 310 statistics:

$$\hat{\mathcal{F}}_{i, \text{unk}}^l = \hat{\sigma}(\mathcal{F}_i^l) \cdot \frac{\mathcal{F}_{i, \text{unk}}^l - \mu(\mathcal{F}_{i, \text{unk}}^l)}{\sigma(\mathcal{F}_{i, \text{unk}}^l)} + \hat{\mu}(\mathcal{F}_i^l). \quad (10)$$

314 Finally, we combine  $\hat{\mathcal{F}}_{i, \text{unk}}^l$  with the original high-frequency part  $\mathcal{F}_{i, \text{unk}}^h$  to form an augmented spec-  
 315 trum  $\hat{\mathcal{F}}(x_{i, \text{unk}}^t)$  and apply inverse DFT to obtain the augmented sample  $\hat{x}_{i, \text{unk}}^t$ . Then, for each  
 316 unknown-category sample  $x_{i, \text{unk}}^t$  and its style-transferred counterpart  $\hat{x}_{i, \text{unk}}^t$ , we extract their feature  
 317 representations:  $z_{i, \text{unk}}^t = f(x_{i, \text{unk}}^t)$ ,  $\hat{z}_{i, \text{unk}}^t = f(\hat{x}_{i, \text{unk}}^t)$ . Let  $\{e_c^{t-1}\}_{c=1}^{C^{t-1}}$  denote the set of known class  
 318 prototypes from the previous stage. For each unknown sample, we convert its cosine similarities  
 319 to these prototypes under both the original and style-transferred views into the *strength parameters*  
 320 of the Plackett–Luce (PL) model:  $\kappa_{i,c} = \exp(\cos(z_{i, \text{unk}}^t, e_c^{t-1}))$ ,  $\hat{\kappa}_{i,c} = \exp(\cos(\hat{z}_{i, \text{unk}}^t, e_c^{t-1}))$ . As  
 321 the number of known classes grows, enumerating or even implicitly handling all  $C^{t-1}!$  permutations  
 322 becomes infeasible. Therefore, following standard practice in listwise ranking (e.g., ListMLE (Xia  
 323 et al., 2008)), we adopt the *factorized* PL likelihood, whose sequential decomposition provides an

analytically exact and computationally tractable form of the model. Given  $\kappa_i = \{\kappa_{i,1}, \dots, \kappa_{i,C^{t-1}}\}$ , the likelihood of a permutation  $\xi$  is:

$$P(\xi \mid \kappa_i) = \prod_{k=1}^{C^{t-1}} \frac{\kappa_{i,\xi(k)}}{\sum_{k'=k}^{C^{t-1}} \kappa_{i,\xi(k')}}, \quad (11)$$

where  $\xi(k)$  denotes the prototype placed at position  $k$ . For illustration, when  $C^{t-1} = 3$  and  $\xi = (a, b, c)$ ,  $P(\xi \mid \kappa_i) = \frac{\kappa_{i,a}}{\kappa_{i,a} + \kappa_{i,b} + \kappa_{i,c}} \cdot \frac{\kappa_{i,b}}{\kappa_{i,b} + \kappa_{i,c}} \cdot \frac{\kappa_{i,c}}{\kappa_{i,c}}$ . This example reflects the inherent sequential normalization of the PL model and does not require constructing or summing over all permutations. To ensure that these associations remain consistent across domains, we enforce view-invariant ranking by aligning the PL likelihoods from the original and style-transferred views through divergence minimization:

$$\mathcal{L}_{\text{rank}} = \frac{1}{N_{t,\text{unk}}} \sum_{i=1}^{N_{t,\text{unk}}} \ell_{\text{KL}}(P(\cdot \mid \kappa_i), P(\cdot \mid \hat{\kappa}_i)), \quad (12)$$

where  $N_{t,\text{unk}}$  denotes the number of unknown-category samples, and  $\ell_{\text{KL}}$  is the Kullback–Leibler divergence. Crucially, the KL divergence between two PL distributions also decomposes into a sum over the corresponding local log-probability terms, meaning that our implementation optimizes the exact computable KL induced by the factorized PL model rather than an approximation over the full permutation space. By enforcing agreement between the two factorized PL likelihoods, the model preserves the *global relative ranking* between unknown samples and known prototypes, providing a strong structure-aware regularization signal for category discovery under domain shift.

### 3.5 ONLINE ADAPTATION

Following the setup of (Park et al., 2024), we assign labels to known and novel samples with different strategies. For data from known categories, we employ the SAM module to generate reliable pseudo-labels. For previously unseen categories, i.e., samples not belonging to any known class, we adopt Affinity Propagation (Frey & Dueck, 2007) to automatically infer cluster memberships. As a non-parametric clustering algorithm, Affinity Propagation iteratively exchanges messages between samples based on pairwise similarities, thereby estimating the optimal number of clusters without requiring it as a prior, which is particularly suitable for open-world scenarios where the number of novel classes is unknown. The inferred clusters are then used to dynamically expand the online classifier, enabling the integration of emerging categories. During online learning, we combine pseudo-labeled known samples with clustered novel samples and incrementally update the model using a standard cross-entropy loss, allowing the system to acquire new semantic knowledge without revisiting past data. The overall optimization objective of our method can be formulated as:  $\mathcal{L}_{\text{total}} = \mathcal{L}_{\text{ce}} + \lambda_1 \mathcal{L}_{\text{rank}}$ , where  $\mathcal{L}_{\text{ce}}$  denotes the cross-entropy loss computed on pseudo-labeled data and  $\lambda_1$  is a balancing hyperparameter.

## 4 EXPERIMENTS

### 4.1 EXPERIMENTAL SETUP

**Dataset** We evaluate our method on two representative benchmarks: the Corrupted Semantic Shift Benchmark (SSB-C) (Wang et al., 2024a) and DomainNet (Peng et al., 2019). SSB-C extends the Semantic Shift Benchmark (SSB) with nine corruption types at five severity levels, covering three fine-grained datasets. This benchmark provides a challenging platform to assess robustness under both semantic and visual perturbations. DomainNet is a large-scale dataset with six diverse domains, featuring hundreds of categories and substantial domain gaps. Following (Wang et al., 2024a), we use the original datasets in SSB-C as known domains and their corrupted versions as unknown domains. For DomainNet, the *Real* domain serves as the known domain, while each of the remaining domains is treated as an unknown domain in turn; we also evaluate a mixed setting where all non-*Real* domains are merged into one unknown domain (details in the Appendix). The category split follows (Cendra et al., 2024): a subset of labeled known classes from the known domain is used in the base session, and subsequent sessions sequentially introduce new streams containing both known and novel categories. Importantly, each session includes samples from both known and unknown domains, simulating realistic scenarios with simultaneous category expansion and domain shift.

378 **Implementation details** We adopt ViT-B/16 (Dosovitskiy et al., 2020) as the backbone, pretrained  
 379 with DINO (Caron et al., 2021; Oquab et al., 2023). Following prior work (Wen et al., 2023; Park  
 380 et al., 2024), only the final transformer block is fine-tuned at each stage using SGD for 30 epochs  
 381 with a batch size of 128. The initial learning rate is 0.1 and decayed to  $1 \times 10^{-4}$  via cosine annealing,  
 382 and weight decay is fixed at  $5 \times 10^{-5}$ . We set the trade-off parameter  $\lambda_1 = 1$ , the number of stages  
 383  $T = 3$ , and the binary mask ratio  $r = 0.3$ . The proximal strength parameter  $\varepsilon$  in the SAM module  
 384 is fixed to 0.5. All experiments are repeated with three random seeds, and averaged results are  
 385 reported. Models are implemented in PyTorch and trained on eight NVIDIA RTX 4090 GPUs.

386 **Evaluation protocol.** We adopt continual clustering accuracy (cACC) (Cendra et al., 2024) as our  
 387 primary evaluation metric. cACC measures the average clustering performance over all sessions up  
 388 to stage  $t$ , defined as:  $cACC_t = \frac{1}{t} \sum_{k=1}^t ACC_k$ . Here,  $ACC_k$  denotes the clustering accuracy on  
 389 the test dataset of session  $k$ . Following (Wang et al., 2024a; Vaze et al., 2022), clustering accuracy  
 390 (ACC) is defined by comparing the ground-truth labels  $y_i$  with the predicted cluster assignments  $\hat{y}_i$ :  
 391  $ACC = \frac{1}{|\mathcal{D}_t^u|} \sum_{i=1}^{|\mathcal{D}_t^u|} \mathbb{I}\{y_i = g^*(\hat{y}_i)\}$ , where  $g^*$  denotes the optimal permutation mapping predicted  
 392 clusters to their ground-truth counterparts. We report cACC results on both known and unknown  
 393 domains, and further break them down into *All*, *Old*, and *New* categories for a comprehensive eval-  
 394 uation.

395 Table 1: Clustering performance on DomainNet benchmark. We use Real as the known domain  
 396 and each of the remaining domains as the unknown domain. We report the average All / Old / New  
 397 accuracy across all stages for both domains.

400	Methods	Real $\rightarrow$ Painting						Real $\rightarrow$ Sketch						Real $\rightarrow$ Quickdraw						Real $\rightarrow$ Clipart						Real $\rightarrow$ Infograph					
		Real			Painting			Real			Sketch			Real			Quickdraw			Real			Clipart			Real			Infograph		
		All	Old	New	All	Old	New	All	Old	New	All	Old	New	All	Old	New	All	Old	New	All	Old	New	All	Old	New	All	Old	New	All	Old	New
GCD	51.3	67.2	45.4	27.4	26.7	28.1	52.3	65.7	41.7	9.2	14.5	10.1	38.7	56.2	29.6	5.0	4.7	5.8	46.7	65.7	40.1	14.5	21.2	10.1	39.8	55.3	32.4	8.1	9.8	6.4	
SimGCD	48.4	63.9	41.3	22.6	22.4	23.5	48.5	60.2	36.5	7.2	11.3	9.2	32.4	50.3	23.5	4.2	4.0	5.1	40.2	58.8	33.5	10.3	18.8	8.2	33.6	49.2	27.8	6.7	7.8	5.2	
SPTNet	49.8	64.5	42.5	24.1	23.5	24.3	49.9	62.3	37.8	7.9	11.7	9.6	34.8	52.6	24.8	4.9	4.6	5.5	43.1	60.3	35.9	11.6	19.3	8.9	35.9	51.4	20.8	7.2	8.0	5.9	
RLCD	50.8	66.2	44.1	25.5	24.6	25.8	51.2	64.8	40.1	8.4	12.1	10.0	36.1	54.0	25.7	4.8	4.7	5.3	45.2	62.1	36.9	13.5	20.9	9.8	37.1	53.2	32.5	8.4	8.9	6.8	
G&M	47.1	62.3	41.2	26.3	25.5	26.2	50.9	63.4	42.3	10.9	15.1	10.5	34.1	50.2	27.3	4.3	4.1	5.2	40.3	61.1	34.2	11.4	19.2	8.8	32.4	50.1	27.6	7.5	9.2	5.5	
Happy	50.6	66.5	44.7	28.0	27.1	28.9	52.0	65.0	41.2	11.2	15.6	10.7	35.6	51.4	28.9	4.6	4.5	5.2	45.6	62.4	37.1	12.0	19.6	9.0	34.2	50.5	28.0	7.9	9.4	5.6	
PA-CGCD	55.4	70.3	48.1	30.1	30.8	30.2	55.1	70.7	46.6	12.6	16.1	11.2	43.6	60.4	34.2	5.1	5.0	6.0	52.2	70.3	44.6	17.8	24.5	12.3	45.2	61.3	38.1	9.0	11.8	7.1	
DEAN	56.0	71.7	47.9	32.8	34.4	31.5	56.7	71.5	47.6	12.9	16.8	11.2	44.0	61.0	35.1	5.3	5.1	6.2	55.1	72.7	47.5	20.3	26.7	15.0	46.7	62.3	40.8	9.5	12.5	7.9	
PromptCCD	56.5	71.2	50.3	31.5	32.1	31.2	57.4	73.6	48.6	13.4	17.7	12.1	45.2	62.3	36.7	5.8	5.1	6.5	54.1	71.2	46.7	19.8	26.1	14.4	47.1	63.1	40.2	9.2	12.2	7.8	
VB-CGCD	57.3	71.0	52.4	32.4	33.6	32.5	56.9	73.1	48.8	13.9	18.1	12.9	47.1	62.1	38.1	6.0	4.9	6.8	55.4	72.0	47.5	19.6	25.8	14.2	48.3	63.9	41.9	9.4	12.4	8.0	
<b>PRISM</b>	<b>60.9</b>	<b>74.1</b>	<b>55.1</b>	<b>39.2</b>	<b>39.0</b>	<b>38.2</b>	<b>60.1</b>	<b>73.4</b>	<b>51.0</b>	<b>16.9</b>	<b>20.1</b>	<b>15.9</b>	<b>54.0</b>	<b>74.0</b>	<b>49.2</b>	<b>7.1</b>	<b>6.5</b>	<b>7.4</b>	<b>58.0</b>	<b>72.3</b>	<b>51.2</b>	<b>24.0</b>	<b>30.4</b>	<b>19.1</b>	<b>60.1</b>	<b>73.8</b>	<b>53.1</b>	<b>10.9</b>	<b>14.1</b>	<b>9.8</b>	

406 Table 2: Clustering performance on SSB-C benchmarks. Each dataset contains both Original and  
 407 Corrupted settings, and we report the average All / Old / New accuracy across all stages for both  
 408 domains.

409	Methods	CUB-C						Stanford Cars-C						FGVC-Aircraft-C					
		Original			Corrupted			Original			Corrupted			Original			Corrupted		
		All	Old	New	All	Old	New	All	Old	New	All	Old	New	All	Old	New	All	Old	New
GCD	29.4	47.7	23.4	26.8	45.9	20.1	26.4	56.1	21.5	22.3	43.1	11.2	27.7	33.6	24.9	28.8	41.4	28.8	
SimGCD	26.6	44.5	21.0	23.4	42.4	17.7	23.1	52.5	18.9	19.3	39.7	9.8	25.4	30.1	22.1	25.2	38.1	25.8	
SPTNet	27.8	45.2	22.0	25.1	44.2	18.1	24.9	55.0	20.3	21.1	41.6	9.9	26.1	31.2	23.3	26.9	39.5	26.7	
RLCD	29.1	46.8	23.8	26.2	45.3	19.4	26.8	56.9	22.1	22.9	43.2	9.7	27.8	32.3	24.2	27.3	40.7	28.1	
G&M	16.4	34.1	10.5	13.7	32.1	7.7	15.7	43.8	12.3	11.4	30.5	6.7	20.5	24.8	17.9	21.6	32.7	22.3	
Happy	22.0	39.4	16.9	19.8	38.4	14.2	21.9	48.7	18.9	18.1	37.0	13.2	24.3	27.9	21.3	24.8	35.6	25.7	
PA-CGCD	28.3	46.5	22.7	25.4	44.7	18.4	25.2	55.1	20.9	21.2	41.5	10.2	26.4	31.4	23.7	27.8	40.1	27.2	
DEAN	28.9	47.1	23.0	26.3	46.2	18.2	26.1	58.1	19.4	22.1	41.2	12.9	28.1	32.8	28.9	29.1	40.1	30.3	
PromptCCD	30.1	48.1	24.5	27.4	46.1	20.3	27.4	57.4	22.1	23.1	44.4	11.4	29.9	34.5	26.4	30.3	42.9	29.9	
VB-CGCD	34.2	51.8	26.3	31.7	49.2	23.4	31.6	59.9	26.1	26.3	47.9	15.1	33.2	37.3	29.7	32.3	44.5	31.6	
<b>PRISM</b>	<b>49.3</b>	<b>64.9</b>	<b>44.2</b>	<b>44.0</b>	<b>60.9</b>	<b>37.0</b>	<b>36.9</b>	<b>60.0</b>	<b>29.1</b>	<b>33.3</b>	<b>56.5</b>	<b>23.5</b>	<b>40.1</b>	<b>48.9</b>	<b>40.1</b>	<b>36.4</b>	<b>46.1</b>	<b>34.1</b>	

## 421 4.2 MAIN RESULTS

422 We compare our method with representative continual discovery baselines, including Grow & Merge  
 423 (G&M) (Zhang et al., 2022), Happy (Ma et al., 2024), PA-CGCD (Kim et al., 2023), DEAN (Park  
 424 et al., 2024), PromptCCD (Cendra et al., 2024), and VB-CGCD (Dai & Chauhan, 2025), as well  
 425 as re-implemented GCD methods (GCD (Vaze et al., 2022), SimGCD (Wen et al., 2023), SPT-  
 426 Net (Wang et al., 2024b) and RLCD (Liu et al., 2025a)). We also note that some recent works,  
 427 such as HiLo (Wang et al., 2024a) and CDAD-Net (Rongali et al., 2024), have explored handling  
 428 distribution shifts in GCD. However, since these methods require access to the entire dataset rather  
 429 than session-based streams, they cannot be directly applied to CCD, and are therefore not included  
 430 in our comparison. Table 1 and Table 2 present the results on the SSB-C and DomainNet bench-  
 431 marks, respectively. It can be observed that in the challenging OW-CCD setting, existing GCD and

432  
433 Table 3: Component-wise ablation on **Real** →  
434 **Painting**.

HCS	SAM	IKT	Real			Painting		
			All	Old	New	All	Old	New
✗	✗	✗	54.6	68.7	46.5	28.7	28.1	27.9
✓	✓	✗	58.1	72.9	49.9	35.0	35.9	32.5
✓	✗	✓	56.9	70.2	52.7	33.2	31.8	35.2
✓	✓	✓	<b>60.9</b>	<b>74.1</b>	<b>55.1</b>	<b>39.2</b>	<b>39.0</b>	<b>38.2</b>

435  
436 Table 4: Comparison of separation strategies on  
437 **Real** → **Painting**.

Methods	Real			Painting		
	All	Old	New	All	Old	New
origin image	55.0	68.7	47.2	29.6	28.9	28.3
entropy-based	54.4	69.0	46.7	29.9	29.1	28.6
energy-based	55.8	69.9	48.1	30.6	29.5	29.9
<b>PRISM</b>	<b>60.9</b>	<b>74.1</b>	<b>55.1</b>	<b>39.2</b>	<b>39.0</b>	<b>38.2</b>

442 CCD approaches struggle to cope with domain shifts, leading to unreliable recognition of known  
 443 classes and poor discovery of new ones. In contrast, our approach consistently achieves more robust  
 444 clustering performance, outperforming both prior CCD and GCD methods by a clear margin. For  
 445 instance, on CUB-C, our method surpasses the strongest CCD competitor, VB-CGCD, by 15.1%  
 446 in the clean domain and 12.3% in the corrupted domain, highlighting its robustness against both  
 447 semantic and visual perturbations. On the more demanding DomainNet benchmark, similar gains  
 448 are observed. For instance, in the **Real** → **Painting** task, PRISM outperforms VB-CGCD by 3.6%  
 449 on the source domain (Real) and 6.8% on the target domain (Painting). These results highlight that  
 450 our approach generalizes effectively to new domains while reliably discovering novel categories in  
 451 continuous streams.

### 452 4.3 ANALYSIS

453 **Effectiveness of different components.** We conduct a comprehensive ablation study to examine  
 454 the contribution of each component in our framework. As shown in Table 3, the baseline performs  
 455 poorly, highlighting the severe impact of domain shifts on both known and novel category recog-  
 456 nition. Incorporating the HCS module to separate known from unknown samples, followed by the  
 457 SAM module, substantially improves clustering accuracy on known categories, confirming the effec-  
 458 tiveness of sparse assignment matching. Introducing the IKT module further enhances the discovery  
 459 of novel categories, underscoring the importance of preserving robust category associations under  
 460 distribution shifts. When all components are integrated, the model achieves the best overall per-  
 461 formance, demonstrating the benefit of combining these modules for reliable open-world continual  
 462 category discovery.

463 **Comparison with alternative separation modules.** To further validate the contribution of the  
 464 HCS module, we carried out a focused ablation study. We compared with three baselines: (1) an  
 465 entropy-driven separation scheme (Safaei et al., 2024), (2) an energy-based approach (Park et al.,  
 466 2024), and (3) a simplified variant of HCS that relies on raw image features without applying fre-  
 467 quency decomposition. As reported in Table 4, the proposed module consistently outperforms these  
 468 alternatives. Its strength lies in exploiting high-frequency information, which preserves more de-  
 469 tailed structural and semantic patterns, allowing the model to more effectively separate unlabeled  
 470 data. This leads to a more reliable basis for recognizing both previously seen and emerging cate-  
 471 gories in continual discovery. In addition, Figure 5 in Appendix provides a qualitative illustration  
 472 of this effect. The HCS module provides a clearer separation between known and unknown groups,  
 473 demonstrating its ability to filter out style-related noise while retaining meaningful semantic  
 474 relations. These observations collectively indicate that HCS is not only beneficial for sample separation  
 475 but also crucial for enhancing overall performance in open-world category discovery under distribu-  
 476 tion shifts.

## 477 5 CONCLUSION

481 In this work, we take the first step toward tackling the challenging problem of open-world continual  
 482 category discovery and introduce three key innovations to address it. First, a high-frequency-driven  
 483 category separation module leverages spectral details to reliably distinguish between known and  
 484 novel categories. Second, a sparse assignment matching module employs proximal optimal trans-  
 485 port to assign trustworthy clustering labels to known classes. Third, an invariant knowledge trans-  
 486 fer module enforces semantic association consistency across domains, enabling robust knowledge

486 transfer under distributional shifts. Extensive experiments on multiple benchmarks validate the ef-  
 487 fectiveness of our framework, demonstrating its ability to consistently recognize known categories  
 488 and uncover new ones in dynamic, non-stationary data streams.  
 489

490 **REFERENCES**  
 491

492 Xinzi Cao, Xiawu Zheng, Guanhong Wang, Weijiang Yu, Yunhang Shen, Ke Li, Yutong Lu, and  
 493 Yonghong Tian. Solving the catastrophic forgetting problem in generalized category discovery.  
 494 In *Proceedings of the IEEE/CVF Conference on Computer Vision and Pattern Recognition*, pp.  
 495 16880–16889, 2024.

496 Mathilde Caron, Hugo Touvron, Ishan Misra, Hervé Jégou, Julien Mairal, Piotr Bojanowski, and  
 497 Armand Joulin. Emerging properties in self-supervised vision transformers. In *Proceedings of*  
 498 *the IEEE/CVF international conference on computer vision*, pp. 9650–9660, 2021.

499 Fernando Julio Cendra, Bingchen Zhao, and Kai Han. Promptccd: Learning gaussian mixture  
 500 prompt pool for continual category discovery. In *European conference on computer vision*, pp.  
 501 188–205. Springer, 2024.

502 Boris Chidlovskii, Stephane Clinchant, and Gabriela Csurka. Domain adaptation in the absence  
 503 of source domain data. In *Proceedings of the 22nd ACM SIGKDD International Conference on*  
 504 *Knowledge Discovery and Data Mining*, pp. 451–460, 2016.

505 Nicolas Courty, Rémi Flamary, and Devis Tuia. Domain adaptation with regularized optimal trans-  
 506 port. In *Joint European conference on machine learning and knowledge discovery in databases*,  
 507 pp. 274–289. Springer, 2014.

508 Hao Dai and Jagmohan Chauhan. Continual generalized category discovery: Learning and forgetting  
 509 from a bayesian perspective. *arXiv preprint arXiv:2507.17382*, 2025.

510 Alexey Dosovitskiy, Lucas Beyer, Alexander Kolesnikov, Dirk Weissenborn, Xiaohua Zhai, Thomas  
 511 Unterthiner, Mostafa Dehghani, Matthias Minderer, Georg Heigold, Sylvain Gelly, et al. An  
 512 image is worth 16x16 words: Transformers for image recognition at scale. *arXiv preprint*  
 513 *arXiv:2010.11929*, 2020.

514 Enrico Fini, Enver Sangineto, Stéphane Lathuilière, Zhun Zhong, Moin Nabi, and Elisa Ricci. A  
 515 unified objective for novel class discovery. In *Proceedings of the IEEE/CVF International Con-*  
 516 *ference on Computer Vision*, pp. 9284–9292, 2021.

517 Rémi Flamary, Nicholas Courty, Davis Tuia, and Alain Rakotomamonjy. Optimal transport for  
 518 domain adaptation. *IEEE Trans. Pattern Anal. Mach. Intell.*, 1(1-40):2, 2016.

519 Brendan J Frey and Delbert Dueck. Clustering by passing messages between data points. *science*,  
 520 315(5814):972–976, 2007.

521 Kai Han, Sylvestre-Alvise Rebuffi, Sébastien Ehrhardt, Andrea Vedaldi, and Andrew Zisserman.  
 522 Autonovel: Automatically discovering and learning novel visual categories. *IEEE Transactions*  
 523 *on Pattern Analysis and Machine Intelligence*, 44(10):6767–6781, 2021.

524 JoonHo Jang, Byeonghu Na, Dong Hyeok Shin, Mingi Ji, Kyungwoo Song, and Il-Chul Moon.  
 525 Unknown-aware domain adversarial learning for open-set domain adaptation. *Advances in Neural*  
 526 *Information Processing Systems*, 35:16755–16767, 2022.

527 Hyungmin Kim, Sungho Suh, Daehwan Kim, Daun Jeong, Hansang Cho, and Junmo Kim. Proxy  
 528 anchor-based unsupervised learning for continuous generalized category discovery. In *Proceed-  
 529 ings of the IEEE/CVF international conference on computer vision*, pp. 16688–16697, 2023.

530 Andreas Krause, Pietro Perona, and Ryan Gomes. Discriminative clustering by regularized infor-  
 531 mation maximization. *Advances in neural information processing systems*, 23, 2010.

532 Wenbin Li, Zhichen Fan, Jing Huo, and Yang Gao. Modeling inter-class and intra-class constraints  
 533 in novel class discovery. In *Proceedings of the IEEE/CVF conference on computer vision and*  
 534 *pattern recognition*, pp. 3449–3458, 2023a.

540 Wuyang Li, Jie Liu, Bo Han, and Yixuan Yuan. Adjustment and alignment for unbiased open set  
 541 domain adaptation. In *Proceedings of the IEEE/CVF Conference on Computer Vision and Pattern*  
 542 *Recognition*, pp. 24110–24119, 2023b.

543 Xiaotong Li, Yongxing Dai, Yixiao Ge, Jun Liu, Ying Shan, and Ling-Yu Duan. Uncertainty mod-  
 544 eling for out-of-distribution generalization. *arXiv preprint arXiv:2202.03958*, 2022.

545 Jian Liang, Ran He, Zhenan Sun, and Tieniu Tan. Distant supervised centroid shift: A simple and  
 546 efficient approach to visual domain adaptation. In *Proceedings of the IEEE/CVF Conference on*  
 547 *Computer Vision and Pattern Recognition*, pp. 2975–2984, 2019.

548 Duo Liu, Zhiqian Tan, Linglan Zhao, Zhongqiang Zhang, Xiangzhong Fang, and Weiran Huang.  
 549 Generalized category discovery via reciprocal learning and class-wise distribution regularization.  
 550 *arXiv preprint arXiv:2506.02334*, 2025a.

551 Hong Liu, Zhangjie Cao, Mingsheng Long, Jianmin Wang, and Qiang Yang. Separate to adapt: Open  
 552 set domain adaptation via progressive separation. In *Proceedings of the IEEE/CVF conference on*  
 553 *computer vision and pattern recognition*, pp. 2927–2936, 2019.

554 Jie Liu, Xiaoqing Guo, and Yixuan Yuan. Unknown-oriented learning for open set domain adapta-  
 555 tion. In *European Conference on Computer Vision*, pp. 334–350. Springer, 2022.

556 Yuanpei Liu, Zhenqi He, and Kai Han. Hyperbolic category discovery. In *Proceedings of the*  
 557 *IEEE/CVF Conference on Computer Vision and Pattern Recognition (CVPR)*, pp. 9891–9900,  
 558 June 2025b.

559 Mingsheng Long, Yue Cao, Jianmin Wang, and Michael Jordan. Learning transferable features with  
 560 deep adaptation networks. In *International conference on machine learning*, pp. 97–105. PMLR,  
 561 2015.

562 Shijie Ma, Fei Zhu, Zhun Zhong, Wenzhuo Liu, Xu-Yao Zhang, and Cheng-Lin Liu. Happy: A  
 563 debiased learning framework for continual generalized category discovery. *Advances in Neural*  
 564 *Information Processing Systems*, 37:50850–50875, 2024.

565 Shijie Ma, Fei Zhu, Xu-Yao Zhang, and Cheng-Lin Liu. Protogcd: Unified and unbiased prototype  
 566 learning for generalized category discovery. *IEEE Transactions on Pattern Analysis and Machine*  
 567 *Intelligence*, 2025.

568 Maxime Oquab, Timothée Darcet, Théo Moutakanni, Huy Vo, Marc Szafraniec, Vasil Khalidov,  
 569 Pierre Fernandez, Daniel Haziza, Francisco Massa, Alaaeldin El-Nouby, et al. Dinov2: Learning  
 570 robust visual features without supervision. *arXiv preprint arXiv:2304.07193*, 2023.

571 Keon-Hee Park, Hakyung Lee, Kyungwoo Song, and Gyeong-Moon Park. Online continuous gen-  
 572 eralized category discovery. In *European Conference on Computer Vision*, pp. 53–69. Springer,  
 573 2024.

574 Xingchao Peng, Qinxun Bai, Xide Xia, Zijun Huang, Kate Saenko, and Bo Wang. Moment matching  
 575 for multi-source domain adaptation. In *Proceedings of the IEEE/CVF international conference*  
 576 *on computer vision*, pp. 1406–1415, 2019.

577 Sai Bhargav Rongali, Sarthak Mehrotra, Ankit Jha, Shirsha Bose, Tanisha Gupta, Mainak Singha,  
 578 Biplob Banerjee, et al. Cdad-net: Bridging domain gaps in generalized category discovery. In *Pro-*  
 579 *ceedings of the IEEE/CVF Conference on Computer Vision and Pattern Recognition*, pp. 2616–  
 580 2626, 2024.

581 Bardia Safaei, VS Vibashan, Celso M De Melo, and Vishal M Patel. Entropic open-set active  
 582 learning. In *Proceedings of the AAAI conference on artificial intelligence*, volume 38, pp. 4686–  
 583 4694, 2024.

584 Kuniaki Saito, Kohei Watanabe, Yoshitaka Ushiku, and Tatsuya Harada. Maximum classifier dis-  
 585 crepancy for unsupervised domain adaptation. In *Proceedings of the IEEE conference on com-*  
 586 *puter vision and pattern recognition*, pp. 3723–3732, 2018a.

594 Kuniaki Saito, Shohei Yamamoto, Yoshitaka Ushiku, and Tatsuya Harada. Open set domain adapta-  
 595 tion by backpropagation. In *Proceedings of the European conference on computer vision (ECCV)*,  
 596 pp. 153–168, 2018b.

597 Swami Sankaranarayanan, Yogesh Balaji, Carlos D Castillo, and Rama Chellappa. Generate to  
 598 adapt: Aligning domains using generative adversarial networks. In *Proceedings of the IEEE*  
 599 *conference on computer vision and pattern recognition*, pp. 8503–8512, 2018.

600 Yuan Shi and Fei Sha. Information-theoretical learning of discriminative clusters for unsupervised  
 601 domain adaptation. *arXiv preprint arXiv:1206.6438*, 2012.

602 Baochen Sun and Kate Saenko. Deep coral: Correlation alignment for deep domain adaptation. In  
 603 *Computer vision–ECCV 2016 workshops: Amsterdam, the Netherlands, October 8–10 and 15–16,*  
 604 *2016, proceedings, part III 14*, pp. 443–450. Springer, 2016.

605 Tao Sun, Cheng Lu, Tianshuo Zhang, and Haibin Ling. Safe self-refinement for transformer-based  
 606 domain adaptation. In *Proceedings of the IEEE/CVF conference on computer vision and pattern*  
 607 *recognition*, pp. 7191–7200, 2022.

608 Eric Tzeng, Judy Hoffman, Ning Zhang, Kate Saenko, and Trevor Darrell. Deep domain confusion:  
 609 Maximizing for domain invariance. *arXiv preprint arXiv:1412.3474*, 2014.

610 Sagar Vaze, Kai Han, Andrea Vedaldi, and Andrew Zisserman. Generalized category discovery.  
 611 In *Proceedings of the IEEE/CVF Conference on Computer Vision and Pattern Recognition*, pp.  
 612 7492–7501, 2022.

613 Enguang Wang, Zhimao Peng, Zhengyuan Xie, Fei Yang, Xialei Liu, and Ming-Ming Cheng. Get:  
 614 Unlocking the multi-modal potential of clip for generalized category discovery. In *Proceedings*  
 615 *of the Computer Vision and Pattern Recognition Conference*, pp. 20296–20306, 2025.

616 Hongjun Wang, Sagar Vaze, and Kai Han. Hilo: A learning framework for generalized category  
 617 discovery robust to domain shifts. *arXiv preprint arXiv:2408.04591*, 2024a.

618 Hongjun Wang, Sagar Vaze, and Kai Han. Sptnet: An efficient alternative framework for generalized  
 619 category discovery with spatial prompt tuning. *arXiv preprint arXiv:2403.13684*, 2024b.

620 Yue Wang, Lei Qi, Yinghuan Shi, and Yang Gao. Feature-based style randomization for domain  
 621 generalization. *IEEE Transactions on Circuits and Systems for Video Technology*, 32(8):5495–  
 622 5509, 2022.

623 Yuzheng Wang, Zhaoyu Chen, Dingkang Yang, Yunquan Sun, and Lizhe Qi. Self-cooperation  
 624 knowledge distillation for novel class discovery. In *European Conference on Computer Vision*,  
 625 pp. 459–476. Springer, 2024c.

626 Xin Wen, Bingchen Zhao, and Xiaojuan Qi. Parametric classification for generalized category dis-  
 627 covery: A baseline study. In *Proceedings of the IEEE/CVF International Conference on Computer*  
 628 *Vision (ICCV)*, pp. 16590–16600, 2023.

629 Yanan Wu, Zhixiang Chi, Yang Wang, and Songhe Feng. Metagcd: Learning to continually learn  
 630 in generalized category discovery. In *Proceedings of the IEEE/CVF International Conference on*  
 631 *Computer Vision*, pp. 1655–1665, 2023.

632 Fen Xia, Tie-Yan Liu, Jue Wang, Wensheng Zhang, and Hang Li. Listwise approach to learning  
 633 to rank: theory and algorithm. In *Proceedings of the 25th international conference on Machine*  
 634 *learning*, pp. 1192–1199, 2008.

635 Renjun Xu, Pelen Liu, Yin Zhang, Fang Cai, Jindong Wang, Shuoying Liang, Heting Ying, and  
 636 Jianwei Yin. Joint partial optimal transport for open set domain adaptation. In *IJCAI*, pp. 2540–  
 637 2546, 2020.

638 Tengyue Xu and Jun Dan. Ehm: Exploring dynamic alignment and hierarchical clustering in unsu-  
 639 pervised domain adaptation via high-order moment-guided contrastive learning. *Neural Networks*,  
 640 185:107188, 2025.

648 Tongkun Xu, Weihua Chen, Pichao Wang, Fan Wang, Hao Li, and Rong Jin. Cdtrans: Cross-domain  
 649 transformer for unsupervised domain adaptation. *arXiv preprint arXiv:2109.06165*, 2021.  
 650

651 Shiqi Yang, Yaxing Wang, Joost Van De Weijer, Luis Herranz, and Shangling Jui. Generalized  
 652 source-free domain adaptation. In *Proceedings of the IEEE/CVF international conference on*  
 653 *computer vision*, pp. 8978–8987, 2021.

654 Xinwei Zhang, Jianwen Jiang, Yutong Feng, Zhi-Fan Wu, Xibin Zhao, Hai Wan, Mingqian Tang,  
 655 Rong Jin, and Yue Gao. Grow and merge: A unified framework for continuous categories discov-  
 656 ery. *Advances in Neural Information Processing Systems*, 35:27455–27468, 2022.

657 Haiyang Zheng, Nan Pu, Wenjing Li, Nicu Sebe, and Zhun Zhong. Textual knowledge matters:  
 658 Cross-modality co-teaching for generalized visual class discovery. In *European Conference on*  
 659 *Computer Vision*, pp. 41–58. Springer, 2024.

660 Zhun Zhong, Linchao Zhu, Zhiming Luo, Shaozi Li, Yi Yang, and Nicu Sebe. Openmix: Reviving  
 661 known knowledge for discovering novel visual categories in an open world. In *Proceedings of the*  
 662 *IEEE/CVF Conference on Computer Vision and Pattern Recognition*, pp. 9462–9470, 2021.

663 Jiaying Zhou and Qingchao Chen. Joint class-level and instance-level relationship modeling for  
 664 novel class discovery. In *Proceedings of the AAAI Conference on Artificial Intelligence*, vol-  
 665 ume 39, pp. 10779–10787, 2025.

## 668 A APPENDIX

### 669 A.1 MORE RELATED WORK

#### 670 A.1.1 CATEGORY DISCOVERY

671 Category discovery aims to transfer knowledge from known classes to identify novel concepts,  
 672 where unlabeled data may contain unseen categories. Novel Class Discovery (NCD) was first in-  
 673 troduced to explore how knowledge from labeled classes can be leveraged to discover entirely new  
 674 ones. Early solutions followed a two-stage strategy. For example, AutoNovel (Han et al., 2021)  
 675 employs self-supervised learning with ranking statistics to transfer knowledge for clustering. Sub-  
 676 sequently, (Fini et al., 2021) proposed a unified end-to-end framework optimizing multiple objec-  
 677 tives simultaneously. IIC (Li et al., 2023a) further model inter-class separability and intra-class  
 678 consistency to improve robustness. OpenMix (Zhong et al., 2021) dynamically mixes labeled and  
 679 unlabeled data to refine pseudo-labels and exploit finer relations among novel classes. While NCD  
 680 assumes that all unlabeled data belong to novel categories, this assumption limits its practicality.  
 681 To address more realistic scenarios, Generalized Category Discovery (GCD) was introduced, where  
 682 the unlabeled pool contains both previously seen and unseen categories. Early GCD methods com-  
 683 bined supervised contrastive objectives with self-supervised representation learning followed by  
 684 semi-supervised clustering (Vaze et al., 2022). Later, SimGCD (Wen et al., 2023) introduced a para-  
 685 metric classifier to improve efficiency and inference speed, establishing a strong baseline. Building  
 686 on these foundations, researchers have proposed a series of more advanced approaches to tackle dif-  
 687 ferent challenges in Generalized Category Discovery. For instance, (Cao et al., 2024) introduced a  
 688 memory-preserving mechanism to alleviate catastrophic forgetting and maintain knowledge of seen  
 689 classes during novel category adaptation. (Liu et al., 2025b) explored hierarchical space modeling,  
 690 arguing that Euclidean or spherical spaces are suboptimal for encoding data with hierarchical struc-  
 691 tures, and instead proposed a hyperbolic embedding space to better capture both seen and unseen  
 692 categories. To unify the treatment of old and new classes, (Ma et al., 2025) developed ProtoGCD,  
 693 which leverages joint prototypes and dual-level pseudo-labeling to balance the recognition of known  
 694 and novel categories while also estimating the number of unseen classes. Beyond the single-domain  
 695 setting, (Wang et al., 2024a) and (Rongali et al., 2024) extended GCD into cross-domain scenarios,  
 696 addressing domain shift by aligning representations across source and target domains with special-  
 697 ized augmentation and adversarial strategies. However, their approaches remain limited to static  
 698 GCD datasets, whereas our work focuses on tackling domain shift under continuous streaming data,  
 699 a setting that more faithfully reflects real-world dynamics. In parallel, multimodal extensions have  
 700 also been explored: (Zheng et al., 2024) proposed TextGCD, a two-phase framework that generates  
 701 descriptive texts via retrieval and employs cross-modality co-teaching, while (Wang et al., 2025)

702 introduced TES, which synthesizes pseudo text embeddings from CLIP to bridge visual and tex-  
 703 tual modalities. Together, these works significantly improve the balance between known and novel  
 704 classes, and continually push the performance boundaries of GCD across both generic and fine-  
 705 grained datasets.

706 Going further, Continuous Category Discovery (CCD) extends GCD to an incremental setting,  
 707 where models continually receive new streams of unlabeled data. The key challenge lies in dis-  
 708 covering new categories while retaining knowledge of past ones. Recent progress in CCD has  
 709 introduced diverse strategies to alleviate forgetting and improve discovery quality. (Zhang et al.,  
 710 2022) presented the Grow-and-Merge framework, which alternates between a growth phase for en-  
 711 riching feature diversity via self-supervised learning and a merging phase that stabilizes recognition  
 712 of previously learned classes. (Wu et al., 2023) proposed a meta-learning optimization approach  
 713 that balances class-discriminative representations for known categories with diverse features for  
 714 novel discovery. (Park et al., 2024) designed DEAN, an online method that performs discovery  
 715 through energy-based guidance and enhances reliability using variance-driven feature augmentation.  
 716 (Cendra et al., 2024) introduced PromptCCD, where Gaussian Mixture Prompting acts as a  
 717 dynamic pool that prevents forgetting and enables adaptive estimation of category numbers. (Dai &  
 718 Chauhan, 2025) developed VB-CGCD, which explains forgetting as covariance misalignment and  
 719 employs variational Bayesian inference with covariance-aware classification to improve robustness  
 720 under noisy pseudo-labels.

721 While these advances move CCD closer to practical continual learning, most methods still rely on the  
 722 simplifying assumption of a fixed domain within each stage. In reality, streaming data often involve  
 723 domain variations or shifts, making such assumptions unrealistic and motivating new frameworks  
 724 that explicitly address multi-domain continual discovery.

725

726

727

728

729

730

731

732

### A.1.2 DOMAIN ADAPTATION

733

734

735

736

737

738

739

740

741

742

743

744

745

746

747

748

749

750

751

752

753

754

755

Domain adaptation seeks to mitigate distribution shifts between a labeled source and a target do-  
 main. A key setting is unsupervised domain adaptation (UDA), which leverages labeled source  
 data and unlabeled target data for model adaptation. UDA methods typically learn domain-invariant  
 representations to reduce distribution shifts. Discrepancy-based approaches minimize statistical dif-  
 ferences between domains via moment-matching techniques (e.g., correlation alignment (Sun &  
 Saenko, 2016) or Maximum Mean Discrepancy (Long et al., 2015; Tzeng et al., 2014)), while ad-  
 versarial approaches (Saito et al., 2018a; Sankaranarayanan et al., 2018) employ domain discrimina-  
 tors to encourage indistinguishable cross-domain features. Recently, Transformer-based backbones  
 (Dosovitskiy et al., 2020) have been explored to enhance feature alignment through attention mech-  
 anisms (Sun et al., 2022; Xu et al., 2021). However, most UDA methods assume joint access to  
 source and target data, which is impractical under privacy constraints. Source-Free Domain Adap-  
 tation (SFDA) addresses this by adapting only a source-trained model with unlabeled target data.  
 (Chidlovskii et al., 2016) suggested using a small set of prototypes instead of the complete source  
 data to facilitate adaptation, while (Liang et al., 2019) enhanced target learning by iteratively refin-  
 ing pseudo-labels through self-training. SHOT (Krause et al., 2010; Shi & Sha, 2012) transfers the  
 source-trained encoder to the target domain by combining information maximization with clustering,  
 keeping the classifier unchanged. To further improve pseudo-label reliability, (Yang et al., 2021) in-  
 troduced neighborhood consistency regularization across target samples. Beyond these transductive  
 settings, researchers have also examined Open-Set Domain Adaptation (OSDA), where target data  
 may involve categories unseen in the source. OSBP (Saito et al., 2018b) introduced a thresholding  
 strategy to separate unknown samples from the known target subset, while STA (Liu et al., 2019)  
 proposed a progressive weighting scheme to gradually disentangle them. More recently, ANNA  
 (Li et al., 2023b) incorporated causal front-door adjustment and decoupled alignment to mitigate  
 semantic bias and enable more reliable transfer under open-set conditions. Although OSDA broad-  
 ens the applicability of domain adaptation, it still mainly focuses on recognizing known categories,  
 while overlooking further exploration of the unknown category space.

756 A.2 THEORETICAL PROOF  
757758 A.2.1 OPTIMIZATION OF SAM  
759760 In this section, we elaborate on the optimization procedure for solving the Sparse Assignment  
761 Matching (SAM) objective. Let  $\psi$  and  $\varphi$  denote the dual variables. The SAM problem can then  
762 be formulated as:

763 
$$\max_{\psi, \varphi} \mathcal{L}_S = \sum_{i=1}^{N_{t, \text{kno}}} \psi_i \hat{a}_i + \sum_{j=1}^{\mathcal{C}^{t-1}} \varphi_j \hat{b}_j - \frac{\varepsilon}{2} \sum_{i=1}^{N_{t, \text{kno}}} \sum_{j=1}^{\mathcal{C}^{t-1}} \left[ \frac{\psi_i + \varphi_j - \tilde{C}_{ij}}{\varepsilon} \right]_+^2, \quad (13)$$
  
764  
765

766 where  $N_{t, \text{kno}}$  denotes the number of known samples,  $\mathcal{C}^{t-1}$  the number of known category prototypes,  
767  $\tilde{C}_{ij} = C_{ij} - \varepsilon \gamma_{ij}^{(l)}$  is the transport cost,  $\hat{a}_i$  and  $\hat{b}_j$  are the corresponding marginals. To efficiently  
768 optimize Eq. equation 13, we adopt the Block Coordinate Descent (BCD) strategy. The updates of  
769 the dual variables are derived by alternatingly fixing one variable and optimizing the other.  
770771 **Update of  $\psi$ .** Taking the derivative of  $\mathcal{L}_S$  with respect to  $\psi_i$  and setting it to zero yields:  
772

773 
$$\Psi(\psi_i) = \sum_{j=1}^{\mathcal{C}^{t-1}} \left[ \psi_i - (\tilde{C}_{ij} - \varphi_j) \right]_+ = \varepsilon \hat{a}_i. \quad (14)$$
  
774  
775

776 **Update of  $\varphi$ .** Similarly, for  $\varphi_j$ , we have:

777 
$$\Phi(\varphi_j) = \sum_{i=1}^{N_{t, \text{kno}}} \left[ \varphi_j - (\tilde{C}_{ij} - \psi_i) \right]_+ = \varepsilon \hat{b}_j. \quad (15)$$
  
778  
779

780 **Update of  $\gamma$ .** With the updated dual variables, the primal transport plan  $\gamma$  can be updated. At the  
781  $l$ -th iteration, the optimal  $\gamma^{(l+1)}$  is obtained as:

782 
$$\gamma_{ij}^{(l+1)} = \max \left( 0, \frac{\psi_i^{(l)} + \varphi_j^{(l)} + \varepsilon \gamma_{ij}^{(l)} - C_{ij}}{\varepsilon} \right), \quad (16)$$
  
783  
784 
$$\tilde{C}_{ij}^{(l+1)} = C_{ij} - \varepsilon \gamma_{ij}^{(l)}.$$
  
785

786 After several iterations, the optimal solutions of  $\psi$  and  $\varphi$  are obtained, based on which the corre-  
787 sponding optimal transport plan  $\gamma$  can be subsequently derived.  
788789 Table 5: Class counts at each incremental stage for the Corrupted SSB and DomainNet benchmarks.  
790 We present the cumulative number of categories in both **Original** and **Corrupted** settings over four  
791 stages.  
792793 

Stage	CUB-C		Stanford Cars-C		FGVC-Aircraft-C		DomainNet	
	Original	Corrupted	Original	Corrupted	Original	Corrupted	Real	Other Domains
0	140	N/A	130	N/A	70	N/A	225	N/A
1	160	160	152	152	80	80	265	265
2	180	180	174	174	90	90	305	305
3	200	200	196	196	100	100	345	345

802 A.2.2 THEORETICAL INTUITION ON DOMAIN INVARIANCE OF HIGH-FREQUENCY CUES  
803804 Given an input image  $x^{(d)} \in \mathbb{R}^{H \times W \times C}$  from domain  $d \in \{s, t\}$ , we apply the discrete Fourier  
805 transform (DFT)  $\mathcal{F}(\cdot)$  and its inverse  $\mathcal{F}^{-1}(\cdot)$ . A binary mask  $M \in \mathbb{R}^{r \times r}$  is constructed to separate  
806 low- and high-frequency components:  
807

808 
$$M_{u,v} = \begin{cases} 1, & \text{if } \max(|u - \frac{H}{2}|, |v - \frac{W}{2}|) \leq r \cdot \frac{\min(H,W)}{2}, \\ 0, & \text{otherwise,} \end{cases} \quad (17)$$
  
809

810  
811  
812  
813  
814  
815  
816  
817  
818  
819  
820  
821  
822  
823  
824  
825  
826  
827  
828  
829  
830  
831  
832  
833  
834  
835  
836  
837  
838  
839  
840  
841  
842  
843  
844  
845  
846  
847  
848  
849  
850  
851  
852  
853  
854  
855  
856  
857  
858  
859  
860  
861  
862  
863  
Table 6: Overview of class partitions in the labeled dataset ( $\mathcal{D}^l$ ) and unlabeled streams ( $\mathcal{D}_1^u$ ,  $\mathcal{D}_2^u$ ,  $\mathcal{D}_3^u$ ), covering both the known and unknown domains.

Class Range	Known Domain				Unknown Domain			
	$\mathcal{D}^l$	$\mathcal{D}_1^u$	$\mathcal{D}_2^u$	$\mathcal{D}_3^u$	$\mathcal{D}^l$	$\mathcal{D}_1^u$	$\mathcal{D}_2^u$	$\mathcal{D}_3^u$
$y_i \in [1, 0.7 \mathcal{C} ]$	87%	7%	3%	3%	0%	7%	3%	3%
$y_i \in (0.7 \mathcal{C} , 0.8 \mathcal{C} ]$	0%	70%	20%	10%	0%	70%	20%	10%
$y_i \in (0.8 \mathcal{C} , 0.9 \mathcal{C} ]$	0%	0%	90%	10%	0%	0%	90%	10%
$y_i \in (0.9 \mathcal{C} ,  \mathcal{C} ]$	0%	0%	0%	100%	0%	0%	0%	100%

and we define

$$\mathcal{F}^l(x) = M \odot \mathcal{F}(x), \quad \mathcal{F}^h(x) = (I - M) \odot \mathcal{F}(x), \quad (18)$$

where  $\odot$  denotes element-wise multiplication. The corresponding spatial components are obtained by

$$x^l = \mathcal{F}^{-1}(\mathcal{F}^l(x)), \quad x^h = \mathcal{F}^{-1}(\mathcal{F}^h(x)). \quad (19)$$

To analyze the domain dependence of different frequency bands, we assume a simple additive decomposition:

$$x^{(d)} = u + v^{(d)}, \quad (20)$$

where  $u$  denotes the domain-shared semantic structure (edges, textures, shapes), and  $v^{(d)}$  represents the domain-specific style (illumination, color tone, or imaging pipeline). In the frequency domain, this becomes

$$\mathcal{F}(x^{(d)}) = \mathcal{F}(u) + \mathcal{F}(v^{(d)}). \quad (21)$$

*Step 1: High-frequency discrepancy is upper-bounded by the high-frequency tail of style.* For the high-pass band  $\Omega_h(r)$  selected by  $(I - M)$ , we have

$$\|\mathcal{F}^h(x^{(s)}) - \mathcal{F}^h(x^{(t)})\|_2 = \|(I - M) \odot (\mathcal{F}(v^{(s)}) - \mathcal{F}(v^{(t)}))\|_2 \leq \|(I - M) \odot \mathcal{F}(v^{(s)})\|_2 + \|(I - M) \odot \mathcal{F}(v^{(t)})\|_2. \quad (22)$$

Since each domain style  $v^{(d)}$  is  $C^m$ -smooth ( $m \geq 1$ ) with bounded Sobolev norm  $\|v^{(d)}\|_{H^m} \leq B$ , then the Fourier energy of its high-frequency tail decays as

$$\int_{\|\omega\| > \rho(r)} |\mathcal{F}(v^{(d)})(\omega)|^2 d\omega \leq C_m \rho(r)^{-2(m-1)} B^2, \quad (23)$$

which implies

$$\|(I - M) \odot \mathcal{F}(v^{(d)})\|_2 \leq C_m^{1/2} \rho(r)^{-(m-1)} B. \quad (24)$$

Substituting into Eq. equation 22, we obtain

$$\|\mathcal{F}^h(x^{(s)}) - \mathcal{F}^h(x^{(t)})\|_2 \leq 2C_m^{1/2} \rho(r)^{-(m-1)} B \equiv \varepsilon(r). \quad (25)$$

As the cutoff frequency  $\rho(r)$  increases,  $\varepsilon(r) \rightarrow 0$ , which means the inter-domain difference in the high-frequency band becomes negligible, and the high-frequency representation is effectively determined by the shared semantics  $u$ .

*Step 2: Low-frequency discrepancy is dominated by style.* For the low-pass band  $\Omega_l(r)$ , we have

$$\|\mathcal{F}^l(x^{(s)}) - \mathcal{F}^l(x^{(t)})\|_2 = \|M \odot (\mathcal{F}(u) - \mathcal{F}(u) + \mathcal{F}(v^{(s)}) - \mathcal{F}(v^{(t)}))\|_2 = \|M \odot (\mathcal{F}(v^{(s)}) - \mathcal{F}(v^{(t)}))\|_2. \quad (26)$$

Since  $\mathcal{F}(v^{(d)})$  concentrates energy near the origin, the right-hand side is non-negligible across domains, showing that low-frequency spectra encode style and illumination variations.

*Step 3: Physical imaging models reinforce this separation.* In practice, cross-domain shifts often arise from: (i) multiplicative/additive low-frequency fields

$$x^{(d)}(p) = a^{(d)}(p)x_{\text{phys}}(p) + b^{(d)}(p), \quad (27)$$

where  $a^{(d)}$  and  $b^{(d)}$  are slowly varying and thus mainly perturb the low-frequency spectrum; and (ii) convolution with smooth kernels  $k^{(d)}$ , whose transfer functions  $K^{(d)}(\omega)$  are low-pass, further

attenuating style at high frequency. Both mechanisms reduce the high-frequency contribution of  $v^{(d)}$  and thus tighten the bound  $\varepsilon(r)$  above.

*Conclusion.* Combining the above derivations and the Fourier decay property yields

$$\|\mathcal{F}^h(x^{(s)}) - \mathcal{F}^h(x^{(t)})\|_2 \leq \varepsilon(r) \rightarrow 0, \quad \|\mathcal{F}^l(x^{(s)}) - \mathcal{F}^l(x^{(t)})\|_2 \rightarrow \text{remains significant} \quad (28)$$

Therefore, high-frequency components  $(I - M) \odot \mathcal{F}(x)$  encode domain-invariant semantic structures, while low-frequency components  $M \odot \mathcal{F}(x)$  capture domain-specific styles. This theoretical analysis explains why the high-frequency cues extracted in Eq.(3) are inherently more robust and domain-invariant in practice.

### A.3 PSEUDOCODE

The pseudocode of PRISM, outlining its main components and training flow, is provided in Algorithm 1.

### A.4 DATASETS

To thoroughly evaluate the proposed framework under both domain shift and semantic shift conditions, we conduct experiments on two widely used benchmarks: **DomainNet** (Peng et al., 2019) and **SSB-C** (Wang et al., 2024a). These datasets encompass diverse visual domains and fine-grained recognition challenges, thereby providing a rigorous test of generalization and robustness.

#### A.4.1 DOMAINNET

DomainNet (Peng et al., 2019) is among the largest benchmarks in domain adaptation and generalization, containing approximately 600,000 images across 345 categories. The dataset spans six heterogeneous domains with distinct visual styles: Real (photographic images), Clipart (cartoon-style drawings), Sketch (hand-drawn sketches), Painting (artistic renderings such as oil and watercolor), Infograph (symbolic infographic-like images), and Quickdraw (doodle-style drawings from Google QuickDraw). The large scale and stylistic diversity introduce strong domain discrepancies, making DomainNet a challenging testbed for algorithms aiming to learn domain-invariant yet discriminative representations.

#### A.4.2 SSB-C

The SSB-C benchmark (Wang et al., 2024a) extends the Semantic Shift Benchmark (SSB) to explicitly measure robustness under semantic and distributional perturbations. The original SSB is built from three fine-grained datasets: CUB-200-2011 (200 bird species with subtle inter-class variations), Stanford Cars (196 categories covering a wide range of brands and models), and FGVC-Aircraft (100 aircraft categories defined by structural differences). SSB-C introduces nine corruption types (e.g., Gaussian noise, frost blur, impulse noise) applied at five severity levels, following the common corruption protocol. This produces a dataset that is nearly **45× larger** than the original SSB, offering a comprehensive benchmark for evaluating robustness in fine-grained recognition.

#### A.4.3 EVALUATION PROTOCOL

For each benchmark, a subset of categories is initially designated as labeled known classes to build the first training session. In subsequent sessions, new categories are gradually introduced, simulating the progressive emergence of novel classes. Detailed statistics of category splits are presented in Table 5, while the proportion of known and unknown samples across unseen domains is summarized in Table 6. These staged splits emulate real-world deployment scenarios in which both novel categories and domain shifts arise over time. Methods are evaluated by their ability to simultaneously recognize known classes and discover unknown ones, with particular emphasis on generalization and semantic separability.

### A.5 COMPREHENSIVE CLUSTERING EVALUATION

To assess both robustness and effectiveness, we perform extensive multi-stage clustering studies on the **SSB-C** and **DomainNet** benchmarks. The summarized outcomes in Tables 7 and 8 report

918  
919  
920

---

921 **Algorithm 1:** PRISM

---

923 **Input** : labeled base set  $\mathcal{D}^l$ ; streaming unlabeled sets  $\{\mathcal{D}_t^u\}_{t=1}^T$ ; model  $\theta = \{f, g\}$ ; mask ratio  $r$ ; SAM  
924 proximal strength  $\varepsilon$ ; rank loss weight  $\lambda_1$

925 **Output:** updated model  $\theta = \{f, g\}$

1 /\* --- High-Frequency-Driven Category Separation (HCS) --- \*/

2 **Function** HCS\_Split( $\mathcal{D}_t^u, f, \{e_c^{t-1}\}, r$ ):

3   **for**  $x \in \mathcal{D}_t^u$  **do**

4     | Compute Fourier spectrum  $\mathcal{F}(x)$  with mask  $M$ ;

5     | Extract high-frequency part  $x^h$ ;

6     |  $S(x) \leftarrow \nu(\max_c \frac{\langle f(x^h), e_c^{t-1} \rangle}{\|f(x^h)\| \|e_c^{t-1}\|})$

7   **end for**

8   Fit 2-comp GMM on  $\{S(x)\}$  and get  $\pi(x)$ ;

9    $\mathcal{D}_{t,kno}^u \leftarrow \{x | \pi(x) \geq 0.5\}$ ,  $\mathcal{D}_{t,unk}^u \leftarrow \{x | \pi(x) < 0.5\}$

10   **return**  $\mathcal{D}_{t,kno}^u, \mathcal{D}_{t,unk}^u$

11 /\* --- Sparse Assignment Matching (SAM) --- \*/

12 **Function** SAM\_Assign( $\mathcal{D}_{t,kno}^u, f, g, \{e_c^{t-1}\}, \varepsilon$ ):

13   Build cost  $C_{ij} = -\log(g(f(x_{i,kno}))_j)$ ;

14   Initialize  $\gamma_{ij}^{(0)}$ ;

15   Solve dual  $(\psi, \varphi)$  and update  $\gamma$  until convergence;

16    $\tilde{y}_i^{kno} \leftarrow \arg \max_j \gamma_{ij}^*$

17   **return**  $\{\tilde{y}_i^{kno}\}, \gamma^*$

18 /\* --- Invariant Knowledge Transfer (IKT) --- \*/

19 **Function** IKT\_RankLoss( $\mathcal{D}_{t,unk}^u, f, \{e_c^{t-1}\}$ ):

20   Estimate low-frequency stats from prev. stage;

21   **for**  $x \in \mathcal{D}_{t,unk}^u$  **do**

22     | Generate style-perturbed view  $\hat{x}$ ;

23     |  $z = f(x), \hat{z} = f(\hat{x})$ ;

24     | Compute PL dists  $P(\mathcal{P}|\kappa), P(\mathcal{P}|\hat{\kappa})$ ;

25     | Accumulate  $\ell_{KL}$

26   **end for**

27    $\mathcal{L}_{rank} \leftarrow$  mean divergence

28   **return**  $\mathcal{L}_{rank}$

29 /\* --- Affinity Propagation + Online Update --- \*/

30 **Function** AP\_Cluster( $\mathcal{D}_{t,unk}^u, f$ ):

31   Run Affinity Propagation on  $\{f(x)\}$ ;

32   **return** novel clusters  $\{\hat{y}^{unk}\}, K_{unk}$

33 **Function** Online\_Update( $\theta, \mathcal{S}_{kno}, \mathcal{S}_{nov}, \mathcal{L}_{rank}, \lambda_1$ ):

34    $\mathcal{L}_{ce} \leftarrow$  cross-entropy on pseudo + novel clusters;

35    $\mathcal{L}_{total} = \mathcal{L}_{ce} + \lambda_1 \mathcal{L}_{rank}$ ;

36   Update model  $\theta = \{f, g\}$ ;

37   **return**  $\theta = \{f, g\}$ , updated prototypes  $\{e_c^t\}$

38 /\* --- Main Procedure --- \*/

39 Initialize  $\theta = \{f, g\}$  and get known-class prototypes  $\{e_c^0\}$  on  $\mathcal{D}^l$

40 **for**  $t = 1$  **to**  $T$  **do**

41   |  $\mathcal{D}_{t,kno}^u, \mathcal{D}_{t,unk}^u \leftarrow$  HCS\_Split( $\mathcal{D}_t^u, f, \{e_c^{t-1}\}, r$ )

42   |  $\{\tilde{y}_i^{kno}\}, \gamma^* \leftarrow$  SAM\_Assign( $\mathcal{D}_{t,kno}^u, f, g, \{e_c^{t-1}\}, \varepsilon$ )

43   |  $\mathcal{L}_{rank} \leftarrow$  IKT\_RankLoss( $\mathcal{D}_{t,unk}^u, f, \{e_c^{t-1}\}$ )

44   |  $\{\hat{y}^{unk}\}, K_{unk} \leftarrow$  AP\_Cluster( $\mathcal{D}_{t,unk}^u, f$ )

45   | Build pseudo-labeled sets  $\mathcal{S}_{kno}, \mathcal{S}_{unk}$ ;

46   |  $\theta, \{e_c^t\} \leftarrow$  Online\_Update( $\theta, \mathcal{S}_{kno}, \mathcal{S}_{unk}, \mathcal{L}_{rank}, \lambda_1$ )

47 **end for**

48 **return** updated model  $\theta = \{f, g\}$

---

969  
970  
971

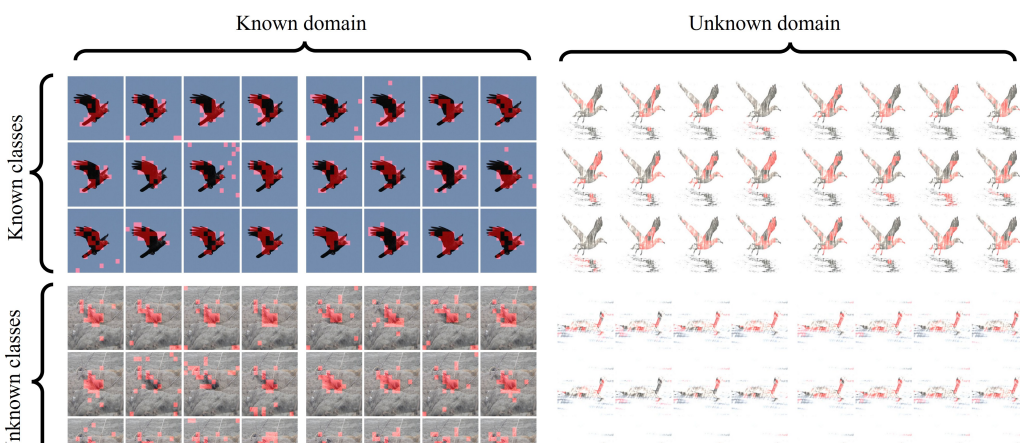
972  
973  
974  
975  
976  
977  
978  
979  
980  
981  
982  
983  
984  
985  
986  
987  
988  
989  
990  
991  
992  
993  
994  
995  
996  
997  
998  
999  
1000  
1001  
1002  
1003  
1004  
1005  
1006  
1007  
1008  
1009  
1010  
1011  
1012  
1013  
1014  
1015  
1016  
1017  
1018  
1019  
1020  
1021  
1022  
1023  
1024  
1025  
Table 7: Clustering results (**mean  $\pm$  std**) on the DomainNet benchmark. The Real domain is treated as the known domain, while each of the other domains serves in turn as the unknown domain. We present the averaged accuracies on All / Old / New classes across all stages for both domains.

Methods	Real $\rightarrow$ Primitive			Real $\rightarrow$ Sketch			Real $\rightarrow$ Quicksilver			Real $\rightarrow$ Object			Real $\rightarrow$ Ingraph			
	All	Real	New	All	Real	New	All	Real	New	All	Real	New	All	Real	New	
ODG	4.7 $\pm$ 2.2	67.2 $\pm$ 3.1	48.4 $\pm$ 1.7	27.4 $\pm$ 1.4	26.7 $\pm$ 1.9	28.7 $\pm$ 1.0	52.7 $\pm$ 1.0	60.7 $\pm$ 1.1	41.7 $\pm$ 1.8	9.2 $\pm$ 0.8	50.7 $\pm$ 2.0	56.2 $\pm$ 2.0	5.0 $\pm$ 0.5	47.4 $\pm$ 0.6	5.9 $\pm$ 0.5	
SimGCD	4.6 $\pm$ 1.7	65.9 $\pm$ 2.3	41.3 $\pm$ 1.1	22.6 $\pm$ 0.9	22.4 $\pm$ 1.3	21.5 $\pm$ 1.3	48.5 $\pm$ 1.0	60.2 $\pm$ 1.2	36.3 $\pm$ 0.9	7.2 $\pm$ 0.9	11.3 $\pm$ 1.2	9.2 $\pm$ 1.2	12.4 $\pm$ 1.6	50.3 $\pm$ 1.2	23.5 $\pm$ 1.0	
SPTNet	4.6 $\pm$ 1.7	65.9 $\pm$ 2.3	41.3 $\pm$ 1.1	22.6 $\pm$ 0.9	22.4 $\pm$ 1.3	21.5 $\pm$ 1.3	48.5 $\pm$ 1.0	60.2 $\pm$ 1.2	36.3 $\pm$ 0.9	7.2 $\pm$ 0.9	11.3 $\pm$ 1.2	9.2 $\pm$ 1.2	12.4 $\pm$ 1.6	50.3 $\pm$ 1.2	23.5 $\pm$ 1.0	
RLCD	80.8 $\pm$ 1.5	66.2 $\pm$ 2.2	44.1 $\pm$ 2.0	25.5 $\pm$ 1.8	24.6 $\pm$ 1.2	25.8 $\pm$ 1.2	51.2 $\pm$ 1.3	60.8 $\pm$ 2.1	40.1 $\pm$ 1.8	8.4 $\pm$ 0.9	11.1 $\pm$ 0.5	10.9 $\pm$ 0.5	8.1 $\pm$ 2.1	54.0 $\pm$ 1.1	25.7 $\pm$ 1.2	
GC&M	8.4 $\pm$ 1.6	70.3 $\pm$ 1.1	46.1 $\pm$ 1.8	20.1 $\pm$ 1.4	20.8 $\pm$ 1.3	20.2 $\pm$ 1.3	55.1 $\pm$ 1.0	70.7 $\pm$ 1.6	46.6 $\pm$ 1.2	12.3 $\pm$ 0.7	16.1 $\pm$ 0.5	12.2 $\pm$ 0.6	4.6 $\pm$ 1.7	60.4 $\pm$ 1.7	12.0 $\pm$ 0.8	
PA-CGCD	8.4 $\pm$ 1.6	70.3 $\pm$ 1.1	46.1 $\pm$ 1.8	20.1 $\pm$ 1.4	20.8 $\pm$ 1.3	20.2 $\pm$ 1.3	55.1 $\pm$ 1.0	70.7 $\pm$ 1.6	46.6 $\pm$ 1.2	12.3 $\pm$ 0.7	16.1 $\pm$ 0.5	12.2 $\pm$ 0.6	4.6 $\pm$ 1.7	60.4 $\pm$ 1.7	12.0 $\pm$ 0.8	
DEAN	50.9 $\pm$ 1.2	71.7 $\pm$ 1.9	47.9 $\pm$ 2.0	22.8 $\pm$ 1.1	34.4 $\pm$ 0.8	15.5 $\pm$ 2.1	56.7 $\pm$ 2.0	71.5 $\pm$ 2.2	47.6 $\pm$ 1.5	10.0 $\pm$ 0.9	11.2 $\pm$ 0.8	44.0 $\pm$ 2.1	61.0 $\pm$ 1.7	5.1 $\pm$ 0.8	51.0 $\pm$ 0.5	6.9 $\pm$ 0.6
Promp-CGCD	37.3 $\pm$ 1.8	71.0 $\pm$ 1.2	52.4 $\pm$ 1.5	22.4 $\pm$ 2.2	33.6 $\pm$ 2.2	25.5 $\pm$ 2.1	56.9 $\pm$ 1.4	70.1 $\pm$ 1.3	48.1 $\pm$ 1.7	12.9 $\pm$ 0.6	18.1 $\pm$ 0.7	47.0 $\pm$ 1.0	62.1 $\pm$ 1.2	55.1 $\pm$ 2.2	47.3 $\pm$ 1.2	
VB-CGCD	34.2 $\pm$ 1.4	51.8 $\pm$ 1.3	26.3 $\pm$ 1.3	31.7 $\pm$ 1.1	49.2 $\pm$ 1.3	23.4 $\pm$ 1.4	51.6 $\pm$ 1.5	59.9 $\pm$ 1.8	27.4 $\pm$ 1.0	20.1 $\pm$ 0.9	20.3 $\pm$ 0.8	47.0 $\pm$ 1.0	50.0 $\pm$ 0.6	13.6 $\pm$ 1.0	37.9 $\pm$ 1.2	
PRISM	50.9 $\pm$ 1.5	74.3 $\pm$ 1.4	56.5 $\pm$ 1.4	20.2 $\pm$ 1.5	39.0 $\pm$ 0.4	28.2 $\pm$ 1.7	50.1 $\pm$ 1.1	70.4 $\pm$ 0.7	34.0 $\pm$ 0.6	10.0 $\pm$ 0.4	10.0 $\pm$ 0.4	50.0 $\pm$ 0.5	74.0 $\pm$ 0.5	34.0 $\pm$ 0.5	70.8 $\pm$ 1.4	

980  
981  
982  
983  
984  
985  
986  
987  
988  
989  
990  
991  
992  
993  
994  
995  
996  
997  
998  
999  
1000  
1001  
1002  
1003  
1004  
1005  
1006  
1007  
1008  
1009  
1010  
1011  
1012  
1013  
1014  
1015  
1016  
1017  
1018  
1019  
1020  
1021  
1022  
1023  
1024  
1025  
Table 8: Clustering results (**mean  $\pm$  std**) on the SSB-C benchmarks. For each dataset, we evaluate on both *Original* and *Corrupted* domains, reporting average accuracies over *All*, *Old*, and *New* categories across different stages.

Methods	CUB-C						Stanford Cars-C						FGVC-Aircraft-C					
	Original			Corrupted			Original			Corrupted			Original			Corrupted		
All	Original	Old	New	All	Old	New	All	Original	Old	New	All	Original	Old	New	All	Original	Old	New
GCD	29.4 $\pm$ 1.4	47.7 $\pm$ 1.5	23.4 $\pm$ 1.5	26.8 $\pm$ 1.3	45.9 $\pm$ 1.5	20.1 $\pm$ 2.2	26.4 $\pm$ 1.0	56.1 $\pm$ 1.8	21.5 $\pm$ 1.7	22.3 $\pm$ 1.0	43.1 $\pm$ 1.0	11.2 $\pm$ 1.6	27.7 $\pm$ 1.0	33.6 $\pm$ 1.2	24.9 $\pm$ 2.1	28.8 $\pm$ 2.2	41.4 $\pm$ 1.4	28.8 $\pm$ 1.8
SimGCD	26.6 $\pm$ 1.5	44.5 $\pm$ 2.0	21.0 $\pm$ 2.1	23.4 $\pm$ 2.0	44.2 $\pm$ 1.2	17.1 $\pm$ 1.2	23.1 $\pm$ 1.6	52.5 $\pm$ 1.4	18.9 $\pm$ 1.1	19.3 $\pm$ 0.8	39.7 $\pm$ 2.2	5.4 $\pm$ 1.5	23.0 $\pm$ 1.6	30.1 $\pm$ 1.6	25.2 $\pm$ 2.0	38.1 $\pm$ 1.0	25.8 $\pm$ 1.4	38.1 $\pm$ 1.4
SPTNet	27.8 $\pm$ 1.3	45.2 $\pm$ 1.5	21.5 $\pm$ 1.8	25.1 $\pm$ 1.2	44.2 $\pm$ 1.2	18.1 $\pm$ 0.8	24.9 $\pm$ 1.7	55.6 $\pm$ 1.3	20.3 $\pm$ 1.3	21.1 $\pm$ 1.1	41.6 $\pm$ 2.0	9.9 $\pm$ 1.0	26.1 $\pm$ 1.7	30.3 $\pm$ 1.6	26.9 $\pm$ 1.7	39.5 $\pm$ 1.6	26.8 $\pm$ 1.7	39.5 $\pm$ 1.6
RLCD	29.1 $\pm$ 1.3	46.8 $\pm$ 1.1	23.8 $\pm$ 1.6	26.2 $\pm$ 1.4	45.3 $\pm$ 1.3	19.4 $\pm$ 1.0	26.8 $\pm$ 1.9	56.9 $\pm$ 1.6	22.1 $\pm$ 1.8	22.9 $\pm$ 1.4	43.2 $\pm$ 1.1	9.7 $\pm$ 1.7	27.8 $\pm$ 1.5	32.3 $\pm$ 1.0	24.2 $\pm$ 1.9	37.3 $\pm$ 1.4	24.2 $\pm$ 1.9	37.3 $\pm$ 1.4
GC&M	10.1 $\pm$ 1.4	47.7 $\pm$ 1.5	23.4 $\pm$ 1.5	22.8 $\pm$ 1.4	47.7 $\pm$ 1.5	18.4 $\pm$ 1.5	25.2 $\pm$ 1.4	55.1 $\pm$ 1.5	20.9 $\pm$ 1.0	21.2 $\pm$ 1.1	41.5 $\pm$ 2.3	10.2 $\pm$ 1.2	26.4 $\pm$ 1.9	12.3 $\pm$ 1.3	45.2 $\pm$ 2.4	10.3 $\pm$ 1.2	38.1 $\pm$ 1.3	45.2 $\pm$ 2.4
PA-CGCD	28.3 $\pm$ 1.7	46.5 $\pm$ 1.6	22.7 $\pm$ 1.8	25.4 $\pm$ 1.2	44.7 $\pm$ 1.9	18.4 $\pm$ 1.6	25.2 $\pm$ 1.9	55.1 $\pm$ 2.2	20.9 $\pm$ 1.0	21.2 $\pm$ 1.1	41.5 $\pm$ 2.3	10.2 $\pm$ 1.2	26.4 $\pm$ 1.3	31.4 $\pm$ 1.7	23.7 $\pm$ 1.6	27.8 $\pm$ 2.2	40.1 $\pm$ 2.3	27.2 $\pm$ 1.2
DEAN	28.9 $\pm$ 1.2	47.1 $\pm$ 2.1	23.0 $\pm$ 1.1	26.3 $\pm$ 1.5	46.2 $\pm$ 2.3	18.2 $\pm$ 1.4	26.1 $\pm$ 1.7	58.1 $\pm$ 1.9	19.4 $\pm$ 0.9	22.1 $\pm$ 1.6	41.2 $\pm$ 1.2	12.9 $\pm$ 2.0	28.1 $\pm$ 1.3	32.8 $\pm$ 1.9	28.9 $\pm$ 1.7	29.1 $\pm$ 2.3	40.1 $\pm$ 2.2	30.9 $\pm$ 1.1
Promp-CGCD	30.1 $\pm$ 1.1	48.1 $\pm$ 1.3	24.5 $\pm$ 1.2	27.4 $\pm$ 1.6	46.1 $\pm$ 1.4	20.3 $\pm$ 1.3	27.4 $\pm$ 1.7	57.0 $\pm$ 2.0	22.1 $\pm$ 1.1	23.1 $\pm$ 1.4	44.9 $\pm$ 1.9	11.4 $\pm$ 1.3	29.9 $\pm$ 1.8	34.5 $\pm$ 1.2	26.4 $\pm$ 2.3	30.3 $\pm$ 1.7	42.9 $\pm$ 2.0	29.9 $\pm$ 1.3
VB-CGCD	34.2 $\pm$ 1.4	51.8 $\pm$ 1.3	26.3 $\pm$ 1.3	31.7 $\pm$ 1.1	49.2 $\pm$ 1.3	23.4 $\pm$ 1.4	31.6 $\pm$ 1.5	59.9 $\pm$ 1.8	26.1 $\pm$ 1.2	26.3 $\pm$ 1.5	47.9 $\pm$ 1.6	15.1 $\pm$ 1.0	30.1 $\pm$ 1.3	37.3 $\pm$ 1.2	29.7 $\pm$ 1.1	32.3 $\pm$ 1.9	44.3 $\pm$ 2.0	31.6 $\pm$ 1.8
PRISM	49.3 $\pm$ 1.2	64.9 $\pm$ 1.3	44.2 $\pm$ 1.3	44.0 $\pm$ 1.2	60.9 $\pm$ 1.5	37.0 $\pm$ 1.0	36.9 $\pm$ 1.5	60.0 $\pm$ 1.0	29.1 $\pm$ 1.4	33.3 $\pm$ 1.4	56.5 $\pm$ 1.0	23.5 $\pm$ 0.9	40.1 $\pm$ 1.1	48.9 $\pm$ 1.1	40.1 $\pm$ 1.4	46.4 $\pm$ 1.3	46.4 $\pm$ 1.2	46.4 $\pm$ 1.2

990  
991  
992  
993  
994  
995  
996  
997  
998  
999  
1000  
1001  
1002  
1003  
1004  
1005  
1006  
1007  
1008  
1009  
1010  
1011  
1012  
1013  
1014  
1015  
1016  
1017  
1018  
1019  
1020  
1021  
1022  
1023  
1024  
1025  
Table 9: Clustering results (**mean  $\pm$  std**) on the DomainNet benchmark under different domain shift scenarios. Table 10 presents evaluations on FGVC-Aircraft-C, Stanford Cars-C, and CUB-C. Such detailed investigations further highlight the strength of our method in reliably identifying novel categories under both distributional changes and sequential learning settings.



1016  
1017  
1018  
1019  
1020  
1021  
1022  
1023  
1024  
1025  
A.6 ATTENTION MAP VISUALIZATION  
To further probe how our model performs spatial reasoning, we inspect the attention distributions of the last transformer block, focusing on the relationship between the [CLS] token and the individual patch tokens across different heads. For each sample, we calculate the attention weights and

1026 Table 9: Stage-wise clustering performance (%) of different methods on the DomainNet benchmark.  
1027 Results are reported for all categories (All), previously known categories (Old), and newly discov-  
1028 ered categories (New) at each incremental stage, along with the overall average.

Methods	Stage 1			Stage 2			Stage 3			Average			Stage 1			Stage 2			Stage 3			Average		
	All	Old	New																					
<i>Real</i>																								
GCD	54.4	70.6	47.7	47.8	63.9	43.1	51.7	67.1	45.4	51.3	67.2	45.4	28.6	28.0	29.3	26.1	25.4	26.8	27.5	26.7	28.3	27.4	26.7	28.1
SimGCD	51.7	66.3	44.1	45.6	61.5	38.4	48.0	63.9	41.4	48.4	63.9	41.3	23.8	23.6	24.7	21.4	21.3	22.3	22.6	22.3	23.5	22.6	22.4	23.5
SPTNet	52.9	67.1	45.3	46.4	61.7	40.0	50.0	64.7	42.1	49.8	64.5	42.5	25.3	24.7	25.8	22.9	22.2	22.9	24.0	23.6	24.3	24.1	23.5	24.3
RLCD	53.3	69.4	46.6	48.5	63.2	41.4	50.7	66.0	44.3	50.8	66.2	44.1	26.7	25.8	27.0	24.2	23.3	24.6	25.6	24.7	25.8	25.5	24.6	25.8
G&M	50.0	66.1	45.0	44.5	58.6	37.4	46.9	62.2	41.2	47.1	62.3	41.2	27.7	26.6	27.3	24.9	24.4	25.1	26.4	25.5	26.2	26.3	25.5	26.2
PA-CGCD	58.1	73.6	50.8	52.8	67.3	45.2	55.3	70.0	48.3	55.4	70.3	48.1	31.3	32.0	31.5	28.8	29.5	29.0	30.2	31.0	30.1	30.1	30.8	30.2
DEAN	58.6	75.1	51.0	52.9	68.3	45.3	56.5	71.7	47.4	56.0	71.7	47.9	33.9	35.8	32.6	31.7	33.0	30.4	32.8	34.4	31.5	32.8	34.4	31.5
PromptCCD	59.1	74.6	53.8	53.9	67.9	47.1	56.5	71.1	50.0	56.5	71.2	50.3	32.7	33.4	32.5	30.2	30.8	29.9	31.6	32.1	31.2	31.5	32.1	31.2
VB-CGCD	60.3	73.1	54.9	54.4	68.8	49.5	57.2	71.1	52.8	57.3	71.0	52.4	33.6	34.9	33.8	31.2	32.4	33.5	32.6	32.4	33.6	32.5	32.4	33.6
PRISM	63.3	76.6	58.9	58.6	71.7	51.4	60.8	74.0	55.0	60.9	74.1	55.1	40.6	40.3	39.6	37.8	37.8	36.9	39.2	38.9	38.1	39.2	39.0	38.2
<i>Real</i> $\rightarrow$ <i>Painting</i>																								
GCD	55.4	69.1	44.0	48.8	62.4	39.4	52.7	65.6	41.7	52.3	65.7	41.7	10.4	15.8	11.3	7.9	13.2	8.8	9.3	14.5	10.3	9.2	14.5	10.1
SimGCD	51.8	62.6	39.3	45.7	57.8	33.6	48.1	60.2	36.6	48.5	60.2	36.5	8.6	12.5	10.4	6.0	10.2	8.0	7.2	11.2	9.2	7.2	11.3	9.2
SPTNet	53.0	64.9	40.6	46.5	59.5	35.3	50.1	62.5	37.4	49.9	62.3	37.8	9.1	12.9	11.1	6.7	10.4	8.2	7.8	11.8	9.6	7.9	11.7	9.6
RLCD	53.7	68.0	42.6	48.9	61.8	37.4	51.1	64.6	40.3	51.2	64.8	40.1	9.6	13.3	11.2	7.1	10.8	8.8	8.5	12.2	10.0	8.4	12.1	10.0
G&M	51.8	67.2	46.1	46.3	59.7	38.5	48.7	63.3	42.3	48.9	63.4	42.3	12.3	16.2	11.6	9.5	14.0	9.4	11.0	15.1	10.5	10.9	15.1	10.5
PA-CGCD	57.8	74.0	49.3	52.5	67.7	43.7	55.0	70.4	46.8	55.1	70.7	46.6	13.5	17.3	12.5	11.0	14.8	10.0	12.4	16.3	11.1	12.3	16.1	11.2
DEAN	59.3	74.9	50.7	53.6	68.1	45.0	57.2	71.5	47.1	56.7	71.5	47.6	14.0	18.2	12.3	11.8	15.4	10.1	12.9	16.8	11.2	12.9	16.8	11.2
PromptCCD	60.0	77.0	52.1	54.8	70.3	45.4	57.4	73.5	48.3	57.4	73.6	48.6	14.6	19.0	13.4	12.1	16.4	10.8	13.5	17.7	12.1	13.4	17.7	12.1
VB-CGCD	59.9	75.2	51.3	54.0	70.9	45.9	56.8	73.2	49.2	56.9	73.1	48.8	15.1	19.4	14.2	12.7	16.9	11.6	13.9	18.0	13.0	13.9	18.1	12.9
PRISM	62.5	75.9	54.8	57.8	71.0	47.3	60.0	73.3	50.9	60.1	73.4	51.0	18.3	21.4	17.3	15.5	18.9	14.6	16.9	20.0	15.8	16.9	20.1	15.9
<i>Real</i> $\rightarrow$ <i>Sketch</i>																								
GCD	41.8	59.6	31.9	39.1	56.1	29.6	35.2	52.9	27.3	38.7	56.2	29.6	6.2	6.0	7.0	5.1	4.7	6.0	3.7	3.4	4.5	5.0	4.7	5.8
SimGCD	35.7	52.7	26.3	32.0	50.3	23.6	29.6	47.9	20.6	32.4	50.3	23.5	5.4	5.2	6.3	4.2	3.9	5.1	3.0	2.9	3.9	4.2	4.0	5.1
SPTNet	37.9	55.2	27.6	35.0	52.8	24.4	31.4	49.8	22.3	34.8	52.6	24.8	6.1	5.8	7.0	4.8	4.7	5.5	3.7	3.3	4.1	4.9	4.6	5.5
RLCD	38.6	57.2	28.2	36.0	53.8	25.9	33.8	51.0	23.0	36.1	54.0	25.7	6.0	5.9	6.5	4.9	4.8	5.3	3.5	3.4	4.1	4.8	4.7	5.3
G&M	37.0	54.0	31.1	33.9	50.1	27.3	31.5	46.5	23.5	34.1	50.2	27.3	4.9	5.2	6.3	3.6	4.1	5.2	2.1	3.0	4.1	3.5	4.1	5.2
PA-CGCD	46.3	63.7	36.9	43.5	60.1	34.4	41.0	57.4	31.3	43.6	60.4	34.2	6.3	6.2	7.3	5.2	5.2	5.9	3.8	3.7	4.8	5.1	5.0	6.0
DEAN	46.6	64.4	38.2	44.5	61.0	34.6	40.9	57.6	32.5	44.0	61.0	35.1	6.2	6.4	7.2	5.1	5.0	6.1	4.0	3.6	5.0	5.1	5.0	6.1
PromptCCD	47.8	65.7	40.2	45.2	62.2	36.4	42.6	59.0	33.5	45.2	62.3	36.7	7.0	6.4	7.8	5.9	5.1	6.5	4.5	3.8	5.2	5.8	5.1	6.5
VB-CGCD	50.1	64.2	40.6	47.0	62.2	38.5	44.2	59.9	35.2	47.1	62.1	38.1	6.8	6.2	7.4	5.6	4.8	6.2	4.4	3.7	4.8	5.6	4.9	6.1
PRISM	56.4	76.5	53.0	53.9	73.9	49.1	51.7	71.6	45.5	54.0	74.0	49.2	8.5	7.8	8.8	7.1	6.4	7.3	5.7	5.3	6.1	7.1	6.5	7.4
<i>Real</i> $\rightarrow$ <i>Quickdraw</i>																								
GCD	41.8	59.6	31.9	39.1	56.1	29.6	35.2	52.9	27.3	38.7	56.2	29.6	6.2	6.0	7.0	5.1	4.7	6.0	3.7	3.4	4.5	5.0	4.7	5.8
SimGCD	35.7	52.7	26.3	32.0	50.3	23.6	29.6	47.9	20.6	32.4	50.3	23.5	5.4	5.2	6.3	4.2	3.9	5.1	3.0	2.9	3.9	4.2	4.0	5.1
SPTNet	37.9	55.2	27.6	35.0	52.8	24.4	31.4	49.8	22.3	34.8	52.6	24.8	6.1	5.8	7.0	4.8	4.7	5.5	3.7	3.3	4.1	4.9	4.6	5.5
RLCD	38.6	57.2	28.2	36.0	53.8	25.9	33.8	51.0	23.0	36.1	54.0	25.7	6.0	5.9	6.5	4.9	4.8	5.3	3.5	3.4	4.1	4.8	4.7	5.3
G&M	37.0	54.0	31.1	33.9	50.1	27.3	31.5	46.5	23.5	34.1	50.2	27.3	4.9	5.2	6.3	3.6	4.1	5.2	2.1	3.0	4.1	3.5	4.1	5.2
PA-CGCD	46.3	63.7	36.9	43.5	60.1	34.4	41.0	57.4	31.3	43.6	60.4	34.2	6.3	6.2	7.3	5.2	5.2	5.9	3.8	3.7	4.8	5.1	5.0	6.0
DEAN	46.6	64.4	38.2	44.5	61.0	34.6	40.9	57.6	32.5	44.0	61.0	35.1	6.2	6.4	7.2	5.1	5.0	6.1	4.0	3.6	5.0	5.1	5.0	6.1
PromptCCD	47.8	65.7	40.2	45.2	62.2	36.4	42.6	59.0	33.5	45.2	62.3	36.7	7.0	6.4	7.8	5.9	5.1	6.5	4.5	3.8	5.2	5.8	5.1	6.5
VB-CGCD	56.7	74.6	50.2	51.5	67.9	43.5	54.1	71.1	46.4	54.1	71.2	46.7	21.0	24.7	15.7	18.5	24.8	13.1	19.9	26.1	14.4	19.8	26.1	14.4
PRISM	58.4	74.1	50.0	52.5	68.9	44.6	55.3	72.1	47.9	55.4	72.0	47.5	20.8	27.1	15.5	18.4	24.6	12.9	19.6	25.7	14.3	19.6	25.8	14.2
PRISM	60.4	74.8	55.0	55.7	69.9	47.5	57.9	72.2	51.1	58.0	72.3	51.2	25.4	31.7	20.5	22.6	29.2	17.8	24.0	30.3	19.0	24.0	30.4	19.1
<i>Real</i> $\rightarrow$ <i>Infograph</i>																								
GCD	42.9	58.7	34.7	40.2	55.2	32.4	36.3	52.0	30.1															

1080 Table 10: Stage-wise clustering accuracy (%) of all methods on FGVC-Aircraft-C, Stanford Cars-C,  
1081 and CUB-C datasets. We report the accuracy on all classes (All), known classes (Old), and novel  
1082 classes (New) at each incremental stage, as well as the average.

Methods	Stage 1			Stage 2			Stage 3			Average			Stage 1			Stage 2			Stage 3			Average		
	All	Old	New																					
<i>FGVC-Aircraft-C</i>																								
GCD	30.8	37.0	27.2	24.2	30.3	22.6	28.1	33.5	24.9	27.7	33.6	24.9	30.0	42.7	30.0	27.5	40.1	27.5	28.9	41.4	29.0	28.8	41.4	28.8
SimGCD	28.7	32.5	24.9	22.6	27.7	19.2	25.0	30.1	22.2	25.4	30.1	22.1	26.4	39.3	27.0	24.0	37.0	24.6	25.2	38.0	25.8	25.2	38.1	25.8
SPTNet	29.2	33.8	26.1	22.7	28.4	20.8	26.3	31.4	22.9	26.1	31.2	23.3	28.1	40.7	28.2	25.7	38.2	25.3	26.8	39.6	26.7	26.9	39.5	26.7
RLCD	30.3	35.5	26.7	25.5	29.3	21.5	27.7	32.1	24.4	27.8	32.3	24.2	29.0	41.9	29.3	26.5	39.4	26.9	27.9	40.8	28.1	27.8	40.7	28.1
G&M	23.4	28.6	21.7	17.9	21.1	14.1	20.3	24.7	17.9	20.5	24.8	17.9	23.0	33.8	23.4	20.2	31.6	21.2	21.7	32.7	22.3	21.6	32.7	22.3
PA-CGCD	29.1	34.7	26.4	23.8	28.4	20.8	26.3	31.1	23.9	26.4	31.4	23.7	29.0	41.3	28.5	26.5	38.8	26.0	27.9	40.3	27.1	27.8	40.1	27.2
DEAN	30.7	36.2	32.0	25.0	29.4	26.3	28.6	32.8	28.4	28.1	32.8	28.9	30.2	41.5	31.4	28.0	38.7	29.2	29.1	40.1	30.3	29.1	40.1	30.3
PromptCCD	32.5	37.9	29.9	27.3	31.2	23.2	29.9	34.4	26.1	29.9	34.5	26.4	31.5	44.2	31.2	29.0	41.6	28.6	30.4	42.9	29.9	30.3	42.9	29.9
VB-CGCD	36.2	39.4	32.2	30.3	35.1	26.8	33.1	37.4	30.1	33.2	37.3	29.7	33.5	45.8	32.9	31.1	43.3	30.3	32.3	44.4	31.7	32.3	44.5	31.6
PRISM	42.5	51.4	43.9	37.8	46.5	36.4	40.0	48.8	40.0	40.1	48.9	40.1	37.8	47.4	35.5	35.0	44.9	32.8	36.4	46.0	34.0	36.4	46.1	34.1
<i>Stanford Cars-C</i>																								
GCD	29.5	59.5	23.8	26.8	56.0	21.5	22.9	52.8	19.2	26.4	56.1	21.5	23.5	44.4	12.4	22.4	43.1	11.4	21.0	41.8	9.9	22.3	43.1	11.2
SimGCD	26.4	54.9	21.7	22.7	52.5	19.0	20.3	50.1	16.0	23.1	52.5	18.9	20.5	40.9	11.0	19.3	39.6	9.8	18.1	38.6	8.6	19.3	39.7	9.8
SPTNet	28.0	57.6	23.1	25.1	55.2	19.9	21.5	52.2	17.8	24.9	55.0	20.3	22.3	42.8	11.4	21.0	41.7	9.9	19.9	40.3	8.5	21.1	41.6	9.9
RLCD	28.7	60.1	24.6	26.1	56.7	22.3	23.9	53.9	19.4	26.2	56.9	22.1	24.1	44.4	10.9	23.0	43.3	9.7	21.6	41.9	8.5	22.9	43.2	9.7
G&M	18.6	47.6	16.1	15.5	43.7	12.3	13.1	40.1	8.5	15.7	43.8	12.3	12.8	31.6	7.8	11.5	30.5	6.7	10.0	29.4	5.6	11.4	30.5	6.7
PA-CGCD	27.9	58.4	23.6	25.1	54.8	21.1	22.6	52.1	18.0	25.2	55.1	20.9	22.4	42.7	11.5	21.3	41.7	10.1	19.9	40.2	9.0	21.2	41.5	10.2
DEAN	28.7	61.5	22.5	26.6	58.1	18.9	23.0	54.7	16.8	26.1	58.1	19.4	23.2	42.6	14.0	22.1	41.2	12.9	21.0	39.8	11.8	22.1	41.2	12.9
PromptCCD	30.0	60.8	25.6	27.4	57.3	21.8	24.8	54.1	18.9	27.4	57.4	22.1	24.3	42.5	12.7	23.2	44.4	11.4	21.8	43.1	10.1	23.1	44.4	11.4
VB-CGCD	34.6	62.0	28.6	31.5	60.0	26.5	28.7	57.7	23.2	31.6	59.9	26.1	27.5	49.2	16.4	26.3	47.8	15.2	25.1	46.7	13.8	26.3	47.9	15.1
PRISM	39.3	62.5	32.9	36.8	59.9	29.0	34.6	57.6	25.4	36.9	60.0	29.1	34.7	57.8	24.9	33.3	56.4	23.4	31.9	55.3	22.2	33.3	56.5	23.5
<i>CUB-C</i>																								
GCD	32.5	51.1	25.7	25.9	44.4	21.1	29.8	47.6	23.4	29.4	47.7	23.4	28.0	47.2	21.3	25.5	44.6	18.8	26.9	45.9	20.3	26.8	45.9	20.1
SimGCD	29.9	46.9	23.8	23.8	42.1	18.1	26.2	44.5	21.1	26.6	44.5	21.0	24.6	43.6	18.9	22.2	41.3	16.5	23.4	42.3	17.7	23.4	42.4	17.7
SPTNet	30.9	47.8	24.8	24.4	42.4	19.5	28.0	45.4	21.6	27.8	45.2	22.0	26.3	45.4	19.6	23.9	42.9	16.7	25.0	44.3	18.1	25.1	44.2	18.1
RLCD	31.6	50.0	26.3	26.8	43.8	21.1	29.0	46.6	24.0	29.1	46.8	23.8	28.4	46.5	20.6	25.9	44.0	18.2	27.3	45.4	19.4	27.2	45.3	19.4
G&M	19.3	37.9	14.3	13.8	30.4	6.7	16.2	34.0	10.5	16.4	34.1	10.5	15.1	33.2	8.8	12.3	31.0	6.6	13.8	32.1	7.7	13.7	32.1	7.7
PA-CGCD	31.0	49.8	25.4	25.7	43.5	19.8	28.2	46.2	22.9	28.3	46.5	22.7	26.6	45.9	19.7	24.1	43.4	17.2	25.5	44.9	18.3	25.4	44.7	18.4
DEAN	31.5	50.5	26.1	25.8	43.7	20.4	29.4	47.1	22.0	27.4	47.6	19.3	25.2	44.8	17.1	26.3	46.2	18.2	26.3	46.2	18.2	27.4	46.1	20.3
PromptCCD	32.7	51.5	28.0	27.5	44.8	21.3	30.1	48.0	24.2	30.1	48.1	24.5	28.6	47.4	21.6	26.1	44.8	19.0	27.5	46.1	20.3	27.4	46.1	20.3
VB-CGCD	37.2	53.9	28.8	31.3	49.6	23.4	34.1	51.9	26.7	34.2	51.8	26.3	32.9	50.5	24.7	30.5	48.0	22.1	31.7	49.1	23.5	31.7	49.2	23.4
PRISM	51.7	67.4	48.0	47.0	62.5	40.5	49.2	64.8	44.1	49.3	64.9	44.2	45.4	62.2	38.4	42.6	59.7	35.7	44.0	60.8	36.9	44.0	60.9	37.0

Table 11: Clustering performance of other DA methods.

Method	Real			Painting		
	All	Old	New	All	Old	New
UOL	55.1	69.0	45.6	29.0	29.3	27.6
Mixstyle	53.2	67.1	44.0	26.0	25.2	25.1
cUADAL	55.7	70.1	46.4	29.9	28.8	26.3
ANNA	54.8	68.4	48.7	30.7	28.9	26.8
PRISM	<b>60.9</b>	<b>74.1</b>	<b>55.1</b>	<b>39.2</b>	<b>39.0</b>	<b>38.2</b>

et al., 2020), class-unknown adversarial adaptation (cUADAL) (Jang et al., 2022), unknown-oriented learning (UOL) (Liu et al., 2022), and the adjustment-and-alignment approach (ANNA) (Li et al., 2023b). The results, summarized in Table 11, show that these methods bring only limited improvements and sometimes even lead to negative transfer, as they focus on distribution alignment but lack the ability to robustly discover novel categories. In contrast, our proposed method consistently outperforms these DA baselines across all benchmarks. The results underscore two key insights: (1) addressing OW-CCD requires going beyond simple domain alignment, by explicitly modeling the interplay between known and unknown categories under evolving distributions; and (2) the proposed design provides a more principled solution tailored for OW-CCD. Taken together, these findings validate the necessity of customizing algorithms for OW-CCD, rather than relying on direct adaptations of existing DA methods.

### A.8 EMPIRICAL STUDY WITH DINOV2 BACKBONE

To further assess the robustness and effectiveness of our proposed framework, we conduct additional experiments using a stronger pretrained backbone, DINOV2, which has recently demonstrated superior representation learning ability in various vision tasks. As shown in Table 12, upgrading the

1134 Table 12: Clustering performance on SSB-C benchmarks using DINOv2 as the backbone. Each  
 1135 dataset includes both Original and Corrupted settings, and we report the average All / Old / New  
 1136 accuracy across all stages for both domains.

1138 1139	Methods	CUB-C						Stanford Cars-C						FGVC-Aircraft-C					
		Original			Corrupted			Original			Corrupted			Original			Corrupted		
		All	Old	New	All	Old	New	All	Old	New	All	Old	New	All	Old	New	All	Old	New
GCD	41.2	55.6	34.9	38.5	53.9	31.5	46.3	65.4	43.4	42.3	53.7	32.3	38.1	39.8	36.1	39.4	49.3	40.4	
SimGCD	39.3	52.4	33.6	35.3	51.4	30.5	42.5	63.3	41.0	39.5	50.0	30.9	36.1	37.4	34.1	36.1	44.2	34.7	
SPTNet	40.5	52.4	34.3	36.9	51.5	30.6	45.0	64.5	41.4	40.4	51.7	32.1	36.0	36.9	31.3	37.8	48.4	36.4	
RLCD	42.4	54.3	35.6	38.3	53.4	32.3	47.1	65.9	43.1	42.1	53.1	34.3	37.8	38.1	33.8	39.3	50.1	38.2	
G&M	28.2	42.6	22.4	25.3	39.3	20.7	36.1	52.8	34.6	30.9	41.0	29.5	31.4	30.9	28.6	31.8	40.3	31.7	
PA-CGCD	40.9	53.8	35.2	38.0	53.2	31.1	45.2	65.6	43.1	40.1	51.6	31.3	38.3	40.2	35.0	37.0	45.7	37.3	
DEAN	41.7	54.5	35.5	37.8	53.6	29.6	45.8	67.4	41.7	41.7	50.8	35.7	40.0	40.2	38.1	38.8	45.6	41.1	
PromptCCD	42.7	55.6	36.0	39.1	54.3	33.2	48.4	67.8	43.7	43.3	53.7	43.1	40.4	42.4	35.9	40.0	48.3	41.0	
VB-CGCD	43.1	56.2	38.1	40.7	55.9	35.9	50.5	<b>68.9</b>	45.7	45.4	56.1	35.3	42.3	43.6	37.8	41.8	49.8	42.5	
<b>PRISM</b>	<b>63.1</b>	<b>73.8</b>	<b>54.9</b>	<b>56.4</b>	<b>71.1</b>	<b>49.8</b>	<b>56.8</b>	<b>68.8</b>	<b>50.1</b>	<b>53.5</b>	<b>67.3</b>	<b>43.2</b>	<b>50.7</b>	<b>56.4</b>	<b>50.1</b>	<b>46.3</b>	<b>51.1</b>	<b>44.7</b>	

1146  
 1147 Table 13: Clustering performance under the setting where multiple domains are treated as unknown.  
 1148 Specifically, we construct the unknown set by combining the five domains from DomainNet except  
 1149 for the Real domain, and report clustering accuracy separately for each domain.

1150 1151	Methods	Real			Painting			Sketch			Quickdraw			Clipart			Infograph		
		All	Old	New	All	Old	New	All	Old	New	All	Old	New	All	Old	New	All	Old	New
		All	Old	New	All	Old	New	All	Old	New	All	Old	New	All	Old	New	All	Old	New
GCD	50.9	66.7	44.9	26.9	26.3	27.7	8.8	14.0	9.6	4.7	2.3	3.6	12.2	20.8	9.7	7.6	9.4	6.0	
SimGCD	48.0	63.5	40.8	22.1	22.1	23.2	6.7	10.9	8.9	3.7	1.6	2.7	8.0	18.3	7.8	6.4	7.4	4.8	
SPTNet	49.4	64.1	42.1	23.7	23.2	24.0	7.6	11.2	9.2	4.5	2.4	3.0	10.3	18.9	8.5	6.9	7.5	5.5	
RLCD	50.5	65.1	43.2	25.0	24.9	25.1	8.1	11.9	10.1	4.3	2.2	2.9	10.6	19.2	8.9	7.2	8.0	5.6	
G&M	46.7	61.9	40.8	25.9	25.1	25.8	10.5	14.7	10.2	3.9	1.8	2.8	10.1	18.7	8.4	7.1	8.7	5.1	
PA-CGCD	55.0	69.9	47.6	29.6	30.4	29.7	11.9	15.7	10.8	4.8	2.5	3.7	15.4	24.1	12.0	8.6	11.4	6.8	
DEAN	55.5	71.2	47.5	32.3	33.9	31.1	12.5	16.4	10.8	5.0	2.6	3.9	18.0	26.3	14.6	9.1	<b>12.9</b>	7.4	
PromptCCD	56.2	70.7	49.8	31.1	31.8	30.8	13.0	17.3	11.7	5.3	2.7	4.2	17.6	25.8	14.0	8.8	11.8	7.4	
VB-CGCD	57.1	71.4	50.3	31.9	32.4	31.7	13.9	18.0	12.4	5.7	3.2	<b>5.1</b>	18.2	26.7	15.1	9.3	12.5	8.2	
<b>PRISM</b>	<b>60.4</b>	<b>73.0</b>	<b>54.8</b>	<b>38.8</b>	<b>39.6</b>	<b>37.8</b>	<b>15.8</b>	<b>19.5</b>	<b>14.9</b>	<b>6.9</b>	<b>5.0</b>	<b>4.9</b>	<b>21.9</b>	<b>29.8</b>	<b>19.3</b>	<b>10.9</b>	<b>12.6</b>	<b>9.3</b>	

1160  
 1161 Table 14: Clustering results on the DomainNet benchmark with extended-stage online discovery. We  
 1162 consider Real as the known domain, while each remaining domain is treated as unknown. Scores  
 1163 are averaged across all stages (including the 4-stage extension) and reported in terms of All / Old /  
 1164 New accuracy for each domain pair.

1165 1166	Methods	Real $\rightarrow$ Painting			Real $\rightarrow$ Sketch			Real $\rightarrow$ Quickdraw			Real $\rightarrow$ Clipart			Real $\rightarrow$ Infograph				
		Real	Old	New	Painting	Old	New	Real	Old	New	Quickdraw	Real	Old	New	Clipart	Real	Old	New
		All	Old	New	All	Old	New	All	Old	New	All	Old	New	All	Old	New	All	Old
GCD	50.9	66.8	44.9	27.8	27.2	28.5	52.8	66.3	42.2	8.7	13.9	9.7	38.1	55.9	29.2	5.4	5.3	6.3
SimGCD	47.9	63.5	40.8	22.9	23.0	24.0	49.0	60.5	36.9	6.7	10.9	8.7	32.1	49.8	23.2	4.5	4.5	5.6
SPTNet	49.3	64.1	42.0	24.5	23.9	24.9	50.4	62.8	38.3	7.6	11.1	9.3	34.3	52.3	24.4	5.3	5.0	6.0
RLCD	49.9	64.8	42.7	25.0	24.3	25.1	51.0	63.3	38.9	8.4	11.9	10.0	35.0	53.1	24.9	5.4	5.1	6.2
G&M	46.7	62.0	40.8	26.7	26.1	26.7	52.3	63.8	42.9	10.5	14.6	10.2	33.6	49.8	26.9	4.8	4.7	5.7
PA-CGCD	55.1	70.0	47.7	30.4	31.3	30.6	55.7	71.1	47.1	11.7	15.6	10.8	43.0	59.9	33.7	5.6	5.3	6.5
DEAN	55.6	71.2	47.6	33.2	34.9	31.9	57.1	72.0	48.2	12.4	16.4	10.6	43.0	60.1	33.7	5.6	5.4	6.6
PromptCCD	56.1	70.8	49.9	31.9	32.6	31.7	58.0	73.9	49.2	13.1	17.4	11.7	44.7	61.9	36.3	6.2	5.5	7.0
VB-CGCD	57.0	71.2	50.3	32.1	33.4	32.4	58.7	<b>74.3</b>	49.9	13.8	18.0	12.1	45.1	62.7	36.9	6.9	5.8	7.3
<b>PRISM</b>	<b>60.8</b>	<b>73.9</b>	<b>54.5</b>	<b>40.1</b>	<b>38.5</b>	<b>39.5</b>	<b>60.7</b>	<b>73.3</b>	<b>52.1</b>	<b>16.3</b>	<b>19.7</b>	<b>15.3</b>	<b>53.3</b>	<b>73.1</b>	<b>48.4</b>	<b>7.3</b>	<b>6.4</b>	<b>7.6</b>

1173 backbone to DINOv2 consistently boosts the performance of all compared algorithms across different  
 1174 benchmarks. This confirms that stronger feature extractors can provide more transferable and  
 1175 discriminative representations for the OW-CCD tasks.

1176 More importantly, under this enhanced backbone setting, our proposed method still achieves the best  
 1177 overall performance and maintains a clear margin over state-of-the-art baselines. This demonstrates  
 1178 that the improvements brought by our framework are orthogonal to backbone advances, and our  
 1179 method continues to deliver substantial gains even when combined with powerful feature extractors.  
 1180 These results highlight the scalability and practical value of our framework when deployed with  
 1181 next-generation backbones such as DINOv2.

### A.9 EVALUATION UNDER MULTIPLE UNKNOWN DOMAINS

1185 To further assess the robustness and practicality of our framework in more complex real-world scenarios, we conduct an additional experiment under a mixed-domain setting. On the DomainNet  
 1186 benchmark, we treat the Real domain as the known domain and merge all the remaining domains  
 1187 (Clipart, Painting, Sketch, and Infograph) into a single unknown domain. Compared

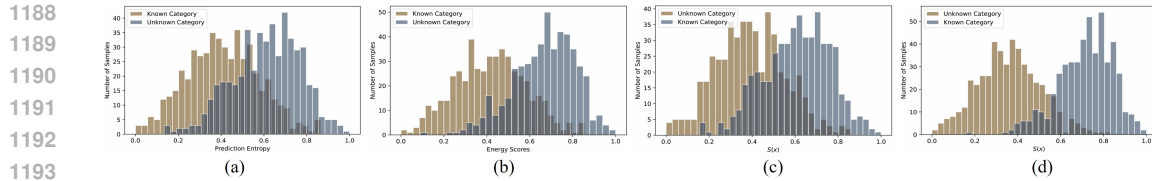


Figure 5: Comparison of different separation strategies.

with single-domain shifts, this mixed-domain setting introduces much greater diversity in both visual styles and semantic structures, making continual category discovery significantly more challenging.

As shown in Table 13, our method consistently outperforms state-of-the-art baselines across all metrics. In particular, we observe notable improvements on novel category discovery, indicating that the proposed approach remains effective even when the unlabeled data come from multiple heterogeneous domains. These results suggest that our framework generalizes well to realistic scenarios where unlabeled streams are inherently multi-sourced and non-stationary.

#### A.10 EVALUATION UNDER MORE-STAGE SETTING

In our main evaluation, we design the online discovery task under a three-phase setting to verify the effectiveness of the proposed framework. To further examine its robustness and scalability under more demanding conditions, we additionally explore a four-phase scenario, where novel categories emerge in a slower and more fragmented manner.

As shown in Table 14, our approach consistently surpasses competitive baselines across all evaluation metrics and category partitions (*All*, *Old*, *New*). These results highlight the framework’s ability to cope with increasingly incremental category arrivals, confirming its adaptability to dynamic and extended discovery processes.

#### A.11 PARAMETER SENSITIVITY ANALYSIS

We further investigate how our method behaves under variations of the loss balancing coefficient  $\lambda_1$ , with results shown in Figure 6 (a)–(b) and (g)–(h). Experiments are conducted on both DomainNet and CUB-C. For DomainNet, the *Real* domain is treated as the known domain and the *Painting* domain as the unknown domain. For CUB-C, we follow the same protocol by designating the *Original* domain as the known domain and the *Corrupted* domain as the unknown domain. By adjusting  $\lambda_1$ , we measure clustering accuracy on all, old, and novel categories within both domains. A clear performance drop is observed when this coefficient is set to zero, highlighting the indispensability of the IKT module. This component aligns listwise ranking distributions between unknown samples and known prototypes before and after spectral perturbation, thereby mitigating spurious style effects and retaining transferable semantic knowledge. More importantly, across a wide range of  $\lambda_1$  values, the accuracy remains consistently high, indicating that our approach is largely insensitive to this parameter and thus robust against hyperparameter tuning.

The mask ratio  $r$  regulates the binary mask  $M$  used to split an image into low- and high-frequency parts, controlling their relative contribution. In our design, high-frequency signals guide the separation of known and novel categories, while low-frequency content is perturbed within the IKT module to encourage transferability. As presented in Figure 6 (c)–(d) and (i)–(j), performance peaks at  $r = 0.3$ , which we adopt as the default setting in all experiments unless stated otherwise. Increasing  $r$  allows the model to exploit richer semantic cues from high-frequency components and enhances robustness of the IKT module by perturbing a broader spectrum of low-frequency information. Nevertheless, when  $r$  becomes excessively large, the model suffers from limited high-frequency cues for separation and over-distortion of semantics within the IKT module, which together harm discriminative ability.

We further conduct a parameter sensitivity analysis on the proximal strength coefficient  $\varepsilon$  in the SAM module. Specifically, we perform experiments on the *Real*  $\rightarrow$  *Painting* domain adaptation scenario, varying  $\varepsilon$  within the range  $\{0.0, 0.01, 0.05, 0.1, 0.5, 1, 10\}$ . As shown in Figure 6 (e)–(f) and

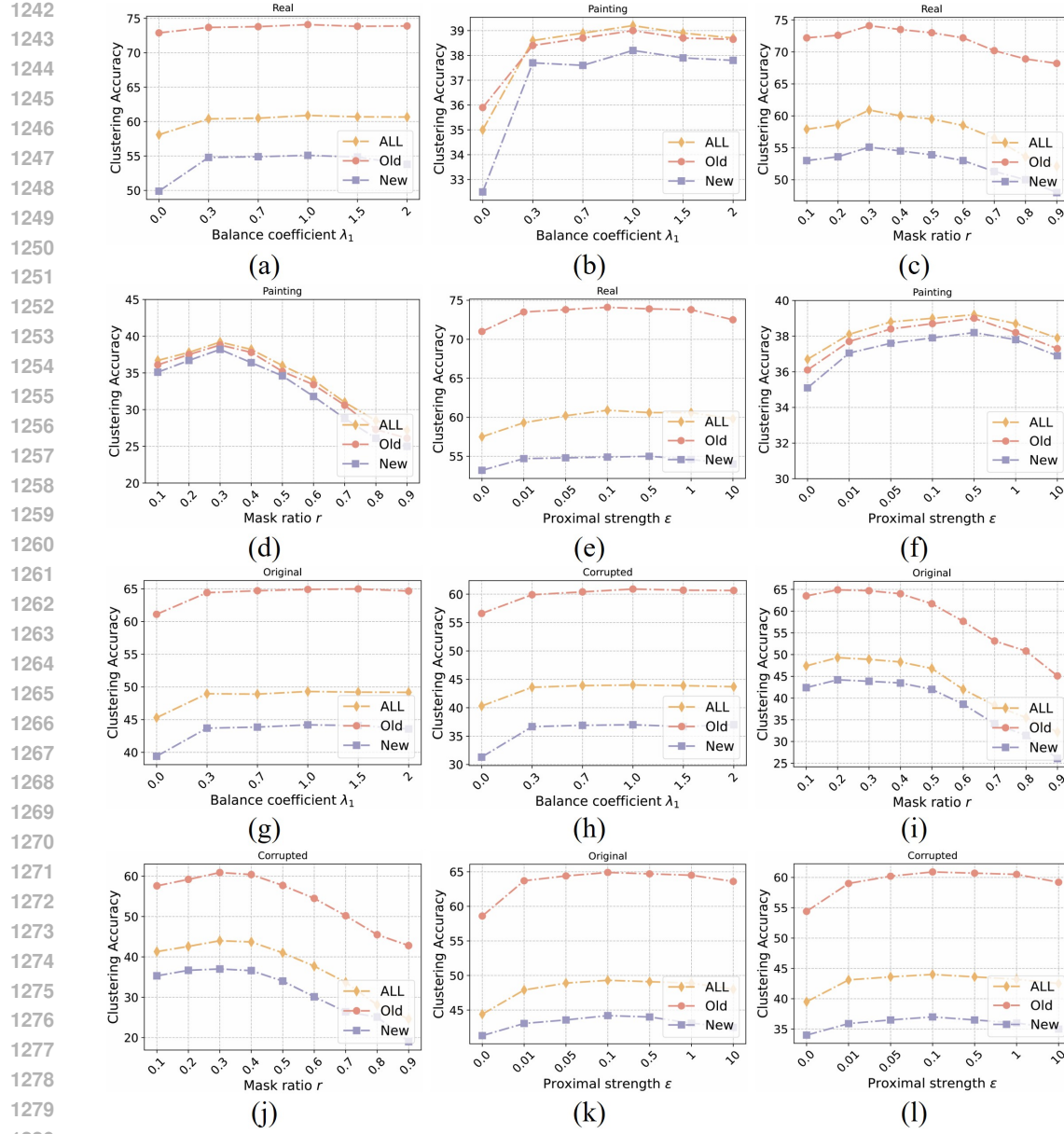


Figure 6: Sensitivity analysis of key hyperparameters.

(k)–(l), the performance of our model remains stable under moderate changes of  $\varepsilon$ . However, when  $\varepsilon$  becomes excessively large, the proximal regularization term dominates over the sparse assignment matching, which may lead to performance degradation. Therefore, we empirically set  $\varepsilon = 0.5$  in all experiments.

#### A.12 COMPUTATIONAL COMPLEXITY ANALYSIS

We profile the computational overhead of each component on an RTX 4090 with batch size 128 and input resolution  $224 \times 224$ . HCS performs one forward DFT/IDFT pair per image (via `torch.fft`), applies a binary frequency-plane mask, runs a cosine-similarity scan against previous-stage prototypes, and fits a 1D GMM on scalar scores; the cost is dominated by FFTs, with masking/cosine/GMM negligible. For the known-like subset, SAM solves a proximal OT subproblem with a few lightweight dual updates over  $(\psi, \varphi)$  and a closed-form refresh of  $\gamma$ ; computing the

cost matrix and sparse projection is minor compared to FFT work. For the unknown-like subset, IKT reuses low-frequency statistics from the previous stage to sample perturbed styles, reconstructs low-frequency spectra and fuses them with the original high-frequency part before an inverse DFT, then compares two feature views (original vs. style-transferred) to all prototypes to build Plackett-Luce listwise distributions and a KL divergence; the extra compute is mainly the single IFFT per unknown sample, with ranking terms lightweight. Overall, the framework adds approximately **5.2 GFLOPs** and increases per-iteration time by  $\sim 0.65$  s, and thanks to GPU-accelerated FFTs, efficient proximal OT updates, and amortized clustering, the overhead remains manageable and scales well to large open-world streams.

Table 15: Stage-wise clustering accuracy (%) of all methods on the CUB-C dataset under the dynamic domain-incremental setting. At each stage, new domains are progressively introduced (Stage 1: Gaussian, Shot, Impulse Noise; Stage 2: Zoom Blur, Snow, Frost; Stage 3: Fog, Speckle, Spatter). We report the accuracy on all classes (All), known classes (Old), and novel classes (New) at each stage, as well as the average across all stages.

Methods	Stage 1			Stage 2			Stage 3			Average			Stage 1			Stage 2			Stage 3			Average		
	All	Old	New																					
<i>CUB-C</i>																								
GCD	31.1	49.4	24.1	28.6	46.2	22.1	24.9	43.2	20.1	28.2	46.3	22.1	23.8	43.0	17.2	26.6	46.0	20.0	25.5	44.5	19.0	25.3	44.5	18.7
SimGCD	28.2	45.1	22.3	24.8	43.0	20.0	22.6	40.9	17.2	25.2	43.0	19.8	20.7	39.8	15.1	23.3	42.4	17.7	22.0	40.9	16.4	22.0	41.0	16.4
SPTNet	29.5	46.0	23.3	26.8	43.9	20.3	23.5	41.1	18.5	26.6	43.7	20.7	22.4	41.3	15.1	25.1	44.1	18.5	23.6	43.0	16.8	23.7	42.8	16.8
RLCD	30.0	48.4	24.6	27.7	45.2	22.7	25.8	42.6	19.9	27.8	45.4	22.4	23.3	42.6	16.6	26.1	45.3	19.3	25.0	44.1	18.1	24.8	44.0	18.0
G&M	17.8	36.4	12.8	14.9	32.7	9.2	12.9	29.3	5.6	15.2	32.8	9.2	10.6	29.6	5.1	13.9	31.8	7.4	12.4	30.7	6.4	12.3	30.7	6.3
PA-CGCD	29.4	48.1	23.9	26.9	44.7	21.6	24.6	42.2	18.7	27.0	45.0	21.4	22.5	41.8	15.7	25.3	44.6	18.5	24.2	43.5	16.8	24.0	43.3	17.0
DEAN	29.9	48.9	24.5	28.2	45.7	21.2	24.8	42.5	19.4	27.6	45.7	21.7	23.7	43.2	15.8	26.1	46.4	18.1	24.8	44.7	16.8	24.9	44.8	16.9
PromptCCD	31.1	49.8	26.4	28.7	46.5	22.8	26.3	43.5	20.1	28.7	46.6	23.1	24.6	43.2	17.4	27.3	46.3	20.4	26.2	44.6	18.8	26.0	44.7	18.9
VB-CGCD	34.7	50.2	27.2	31.9	48.5	25.4	29.3	46.5	22.4	32.0	48.4	25.0	26.9	45.4	19.5	29.6	48.4	22.4	28.4	46.6	21.1	28.3	46.8	21.0
PRISM	<b>51.1</b>	<b>66.7</b>	<b>47.6</b>	<b>48.9</b>	<b>64.4</b>	<b>43.9</b>	<b>47.0</b>	<b>62.4</b>	<b>40.5</b>	<b>49.0</b>	<b>64.5</b>	<b>44.0</b>	<b>41.9</b>	<b>59.1</b>	<b>35.1</b>	<b>45.1</b>	<b>61.9</b>	<b>38.2</b>	<b>43.6</b>	<b>60.2</b>	<b>36.5</b>	<b>43.5</b>	<b>60.4</b>	<b>36.6</b>

### A.13 EXPERIMENTS ON DYNAMIC DOMAIN-INCREMENTAL SETTING

To further evaluate the performance of our proposed algorithm in dynamic domains, we conducted an additional domain-incremental experiment. Specifically, we trained on the CUB-C dataset over three stages, where new domains were progressively introduced at each stage. In Stage 1, we introduced three types of perturbations: Gaussian Noise, Shot Noise, and Impulse Noise. In Stage 2, we further incorporated Zoom Blur, Snow, and Frost. In Stage 3, additional perturbations including Fog, Speckle, and Spatter were introduced. In this way, we simulated a realistic dynamic and non-stationary data stream scenario, where each stage may involve domains unseen in the previous stage. As shown in Table 15, we observed that under this more challenging dynamic-domain setting, our model still achieved significant performance improvements and substantially outperformed other competing methods, further demonstrating the robustness and effectiveness of the proposed approach.

### A.14 VISUALIZATION OF HCS SEPARATION ACROSS FINE-GRAINED DATASETS

We further visualize the separation behavior of HCS on several fine-grained datasets, as illustrated in Fig. 7. Across most datasets, the separation scores of known and unknown samples show a certain degree of discrepancy, indicating that HCS can reliably distinguish the two groups using high-frequency information. Even on challenging fine-grained benchmarks—such as Stanford Cars-C—where categories share strong visual resemblance, the score distributions still exhibit an approximate bimodal pattern, demonstrating that meaningful separation can be achieved.

These observations highlight two important facts. First, high-frequency cues consistently provide better separation than raw images, as the removal of low-frequency domain biases makes the remaining semantic differences more distinguishable. Second, although the separability on fine-grained datasets is naturally reduced due to subtle inter-class variations, high-frequency decomposition still improves the separation of known and unknown samples.

Overall, the results in Fig. 7 confirm that high-frequency cues offer more reliable and robust separation than original images across diverse datasets, including challenging fine-grained scenarios.

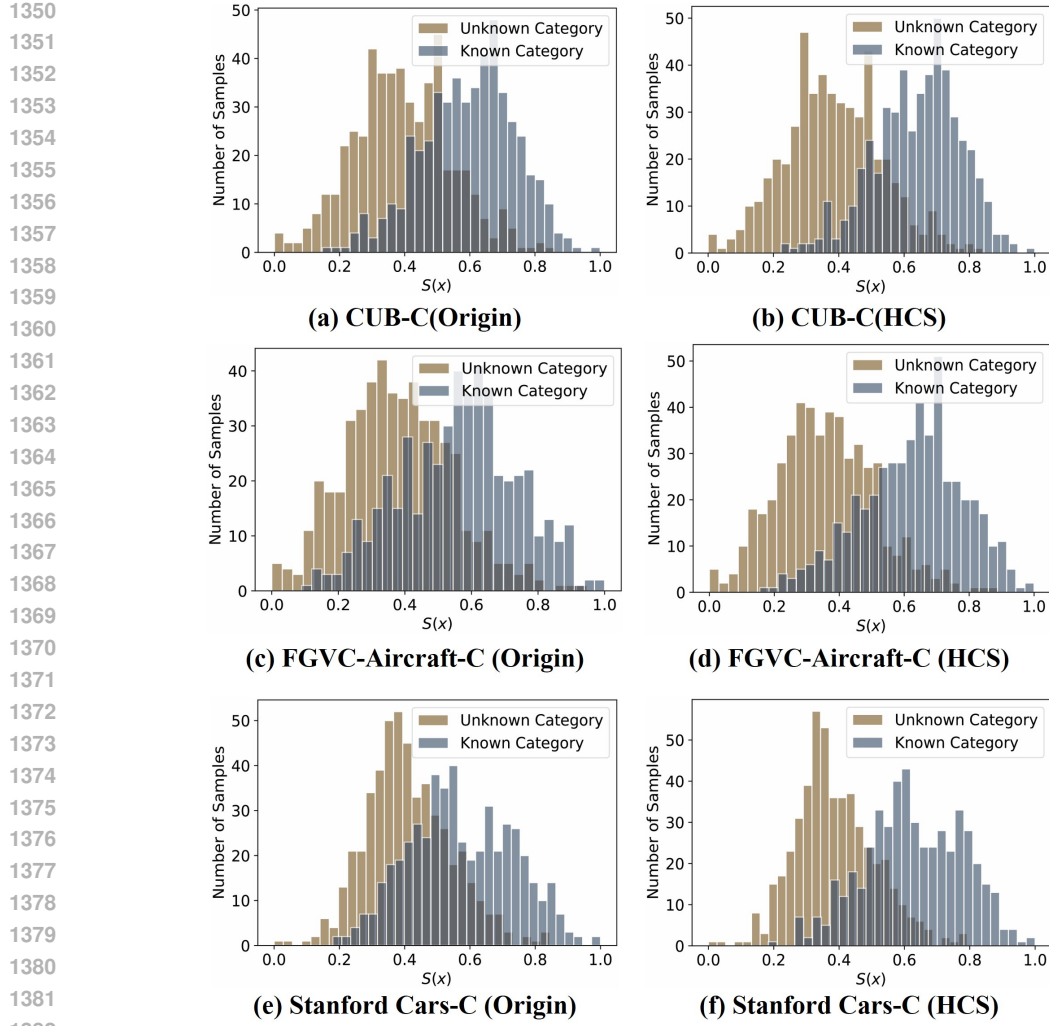


Figure 7: Comparison of separation performance across multiple fine-grained datasets.

### A.15 BAD CASE ANALYSIS

Although the proposed HCS module provides robust separation between known and unknown samples across diverse datasets and corruption types, certain challenging scenarios may still lead to reduced performance. A representative example arises under structural blurring—such as zoom blur—which directly suppresses the semantic high-frequency cues that HCS relies on.

Structural blur smears object boundaries, attenuates fine textures, and destroys edge sharpness, thereby weakening the discriminative high-frequency structures essential for our separation mechanism. As illustrated in Appendix Fig. 8, the extracted high-frequency representations become less informative in these cases, causing the separation scores of known and unknown samples to move closer.

Nevertheless, even under such challenging corruptions, HCS consistently outperforms using raw images. This is because the high-frequency decomposition still removes domain-specific low-frequency biases, and the preserved semantic structures—although partially degraded—remain more discriminative than full-spectrum representations. The resulting separation curve demonstrates that the degradation introduced by structural blur affects both HCS and raw images, but the impact is notably smaller for HCS.

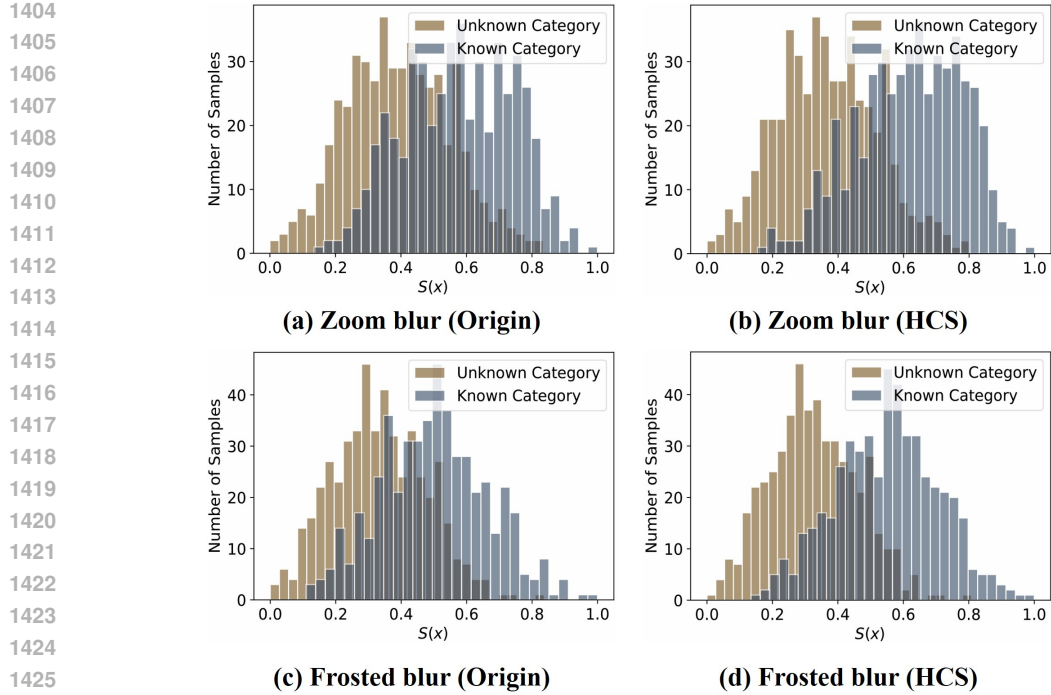


Figure 8: Illustration of a challenging case, where structural blurring suppresses semantic high-frequency cues and weakens separation, yet HCS still outperforms raw-image representations.

Table 16: Clustering results of various methods on the DomainNet benchmark. Each experiment uses *Real* as the source domain, with one of *Painting*, *Sketch*, *Quickdraw*, *Clipart*, or *Infograph* serving as the target. Clustering accuracy is reported for both domains.

Methods	Real + Painting			Real + Sketch			Real + Quickdraw			Real + Clipart			Real + Infograph		
	All	Old	New	All	Old	New	All	Old	New	All	Old	New	All	Old	New
CDAD-Net	63.6	<b>77.9</b>	56.3	38.4	38.4	37.5	61.9	76.3	52.1	17.3	20.9	15.9	48.5	66.5	36.7
HiLo	64.4	77.6	57.5	42.1	42.9	41.3	63.3	77.9	55.9	19.4	22.4	17.1	58.6	76.4	52.5
PRISM	<b>68.7</b>	77.8	<b>63.3</b>	<b>47.2</b>	<b>46.8</b>	<b>45.8</b>	<b>68.7</b>	<b>78.2</b>	<b>63.0</b>	<b>23.8</b>	<b>24.9</b>	<b>22.8</b>	<b>61.8</b>	<b>77.5</b>	<b>57.1</b>

Overall, these bad cases highlight an inherent limitation: when corruptions significantly destroy semantic high-frequency content, the separability achievable by HCS naturally decreases. This observation suggests a promising future direction—integrating structure-preserving or deblurring techniques to further enhance the robustness of high-frequency-based separation under severe image degradations.

#### A.16 COMPARISON WITH EXISTING DOMAIN-SHIFT GCD METHODS

Although prior domain-shift GCD approaches such as HiLo Wang et al. (2024a) and CDAD-Net Rongali et al. (2024) cannot be directly adapted to the same *domain-shift + CCD* setting considered in our work, our framework can still be applied to the standard cross-domain GCD scenario for fair comparison. Following the experimental protocol of HiLo, we evaluate our method alongside HiLo and CDAD-Net under the cross-domain GCD setting (note that this is *not* the proposed OW-CCD scenario). As shown in the results, our approach outperforms both HiLo and CDAD-Net in most cases, demonstrating that the proposed method is flexible and effective even when applied to conventional cross-domain GCD tasks.

#### A.17 SOCIETAL IMPACT AND FUTURE DIRECTIONS

We study Open-World Continual Category Discovery (OW-CCD), which reflects the reality of dynamic data streams where category distributions are non-stationary and new classes emerge over time. This research has broad societal implications, as it equips AI systems to adaptively recog-

1458 Table 17: Clustering results of various methods on the SSB-C benchmark. For each dataset (CUB,  
 1459 Scars, and FGVC), the clean set serves as the source domain, while its corrupted counterpart is  
 1460 treated as the target domain. Clustering accuracy is reported for both domains.

Methods	CUB-C						Scars-C						FGVC-C					
	Original			Corrupted			Original			Corrupted			Original			Corrupted		
	All	Old	New															
CDAD-Net	40.4	38.9	39.3	37.7	39.1	34.2	32.1	42.9	32.2	28.8	35.6	21.4	33.8	35.5	31.2	27.8	29.6	25.6
HiLo	56.8	54.0	60.3	52.0	53.6	50.5	39.5	44.8	37.0	35.6	42.9	28.4	44.2	50.6	47.4	31.2	29.0	33.4
PRISM	<b>60.1</b>	<b>58.7</b>	<b>63.1</b>	<b>56.2</b>	<b>55.1</b>	<b>54.9</b>	<b>44.0</b>	<b>47.4</b>	<b>40.6</b>	<b>40.1</b>	<b>43.5</b>	<b>34.5</b>	<b>47.9</b>	<b>55.1</b>	<b>51.8</b>	<b>35.7</b>	<b>31.8</b>	<b>39.1</b>

1467  
 1468 nize evolving concepts in real-world scenarios such as medical diagnostics, ecological monitoring,  
 1469 and social media moderation, thereby enhancing their reliability and fairness in open environments.  
 1470 However, limitations remain: (1) the open world introduces vast distributional shifts and complex  
 1471 dynamics, where current models still struggle to maintain stable performance; and (2) most existing  
 1472 work relies on single-modality data, whereas extending to multi-modal OW-CCD is crucial to fully  
 1473 exploit diverse real-world signals (e.g., combining image, text, and sensor data) for robust knowl-  
 1474 edge discovery. These challenges highlight promising future directions, motivating research into  
 1475 more resilient algorithms and multi-modal learning frameworks for open-world continual discovery.

#### 1476 A.18 ETHICS STATEMENT

1477 This research does not involve human participants, animal subjects, or the use of sensitive personal  
 1478 data, nor does it present any potentially harmful applications. All experiments are conducted on  
 1479 publicly available benchmark datasets that are properly licensed for academic use. The authors are  
 1480 committed to adhering to ethical research standards and to promoting fairness, transparency, and  
 1481 responsible development of AI technologies.

#### 1482 A.19 USE OF LLMs

1483 During the preparation of this manuscript, we made limited use of publicly available large language  
 1484 models (LLMs) solely to assist with English writing. All technical content, including the formulation  
 1485 of ideas, design of methodologies, implementation of experiments, and interpretation of results, was  
 1486 entirely conceived and written by the authors without LLM involvement. The role of LLMs was  
 1487 strictly confined to stylistic and linguistic improvements, comparable to grammar- or spell-checking  
 1488 software. No novel research insights, data, or analyses were generated by LLMs, and all scientific  
 1489 claims and results presented in this work remain the sole responsibility of the authors.

#### 1490 A.20 REPRODUCIBILITY

1491 To ensure reproducibility, we provide a comprehensive description of the model design in Section 3  
 1492 and detailed experimental settings in Section 4.1. Furthermore, we include the full pseudocode of the  
 1493 proposed PRISM framework in Appendix A.3, clearly outlining its main components and training  
 1494 flow. These details collectively enable faithful reimplementations and verification of our results.

1495  
 1496  
 1497  
 1498  
 1499  
 1500  
 1501  
 1502  
 1503  
 1504  
 1505  
 1506  
 1507  
 1508  
 1509  
 1510  
 1511